Dear Jim Haywood,

Thank you for your positive review of our manuscript. We appreciate the comments and suggestions you provided and we believe they will greatly improve the clarity and scientific robustness of the manuscript. Below we have provided responses (in boldface) to each of the major and minor comments. Line numbers refer to the revised manuscript.

Note: the color coding for the edit markings in the document are as follows:
Blue: directly addresses a comment from Reviewer #1 (you)
Green: directly addresses a comment from Reviewer #2 (anonymous)
Red: additional update made by Authors

Review of Cochrane et al, AMT

This paper builds on the previous work of Cochrane et al. (2019) and examines the direct radiative effect of biomass burning aerosols over cloudy and clear-sky conditions during the ORACLES 2016 and 2017 measurement campaigns. There are three main aspects: 1) assessing the aerosol optical parameters that give consistent radiative closure, 2) developing a basic and extended algorithm that parameterizes the DARE as a function of the scene albedo and the optical depth (at 550 nm) and 3) adding an additional dependency on SSA.

I was very interested and impressed by the SSA retrievals when compared to some of the more accurate assessments of SSA that are now possible using more advanced instrumentation (e.g. airborne CRD and PAS measurements that are not subject to the artefacts associated with missing scattering (nephelometers) or with scattering/absorption artefacts (filter based absorption measurements). I have included some additional references to these measurements as they were not included by the authors – I do think that these complementary studies provide excellent additional supporting information for the validity of the approach.

The second part of the paper which documents the performance of the P_DARE and PX_DARE could certainly be of use when compared to satellite data, but one would have to have an estimate of the above cloud/above surface AOD and the scene albedo. The most obvious place where this could have applicability might therefore be a combination of e.g. space borne lidar and broadband scene albedo from e.g. GERB; it might be worth explicitly stating this as a future possibility.

I deal with the comments as more major and minor below.

More Major:

Point 1: L325 onwards: It is worth emphasizing that many of the in-situ retrievals of SSA have, in the past and in the ORACLES measurements, relied on filter based measurements for absorption and nephelometers for scattering (authors' Figure 4). These instruments have relatively large uncertainties associated with them because of corrections needed for scattering and absorbing artefacts (e.g. Cappa et al., 2008). Much more accurate measurement systems such as Cavity Ring Down (extinction) and Photo Acoustic Spectrometry have been developed.

Cappa, C. D., Lack, D. A., Burkholder, J. B., and Ravishankara, A. R.: Bias in filter-based aerosol light absorption measurements due to organic aerosol loading: Evidence from laboratory measurements, Aerosol Sci. Technol., 42, 1022–1032, https://doi.org/10.1080/02786820802389285, 2008.

I know that it is difficult to keep up with the contemporary literature, particularly with the concentrated efforts over the SE Atlantic region, but there is some recent work from the CLARIFY- 2017 team that very much supports the values of the SSA (and the wavelength dependence). I would suggest adding something like this:-

"New, more accurate, cavity ring down and photo acoustic spectrometry instrumentation has recently been deployed to the SE Atlantic during the CLARIFY-2017 deployment. Davies *et al*. (2019) performed an analysis of the SSA of aerosol dominated by biomass burning aerosol using such instrumentation and found mean SSA values of 0.84, 0.83 and 0.81 at interpolated wavelengths of 467, 528, and 652 nm respectively. Wu *et al*. (2020a) extended this analysis by examining the BBA in the free troposphere, finding a mean and variability in BBA SSA of 0.85 ± 0.02 (1stdev) and 0.82±0.04 (1stdev) at 405 and 658 nm with evidence that the BBA at higher altitudes in the free troposphere is less absorbing. These results appear entirely consistent with those derived here."

The authors should consider including a combination of the Davies et al. (2019)/Wu et al. (2020) paper on their Figure 4 as the agreement is so good.....Of course, you would have to caveat this with the fact that there are different temporal and geographical sampling regions etc.

Thank you for these comments. We apologize for our unintentional exclusion of the other SEA campaigns beyond ORACLES. We have included the suggested text on line 374. In figure 4, we have added an additional indicator of the Davies et al., 2019 results. We choose not to include the Wu et al., 2020 results since the wavelengths are not as similar.

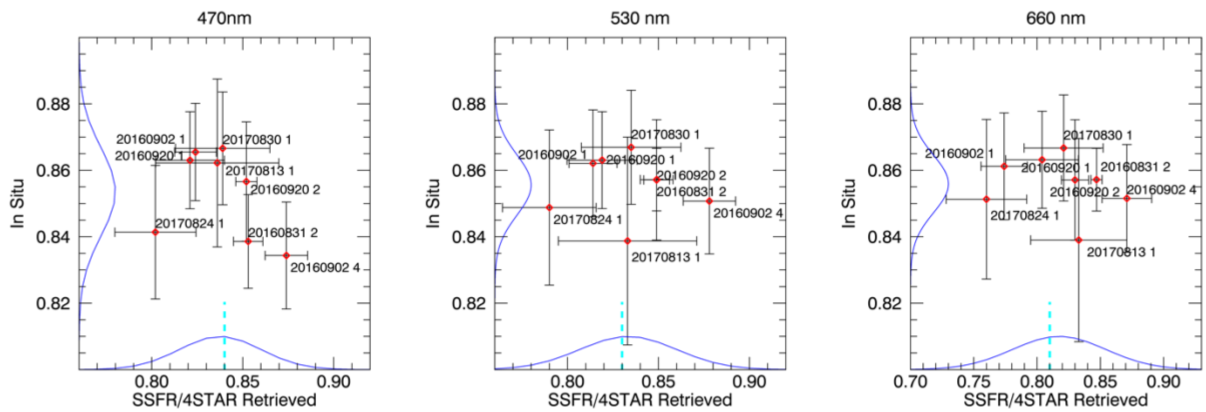

Point 2: Line 234. The RT calculations themselves have a degree of uncertainty associated with them. For example, I note that the aerosol is characterized by the asymmetry factor. Does this mean that the higher order moments of the phase function are not accounted for? Is the RT code 2-stream? Is delta-Eddington rescaling applied? How is the surface reflectance modelled? A few more details would be appropriate here as would some acknowledgement that radiative transfer models that treat aerosols have their own inherent uncertainty (e.g. Boucher et al., 1999).

Thank you for pointing out the lack of detail surrounding the RT calculations within the manuscript. The RT calculations are performed with a multi stream RT model, disort (run with 6 streams). There is no delta-Eddington rescaling. The model assumes a Henyey-Greenstein (HG) phase function with our retrieved asymmetry parameter as input for the DARE calculations. We do not at all claim here that HG is, in fact, the actual phase function. On the contrary, the real phase function most likely deviates from HG significantly. However, since we retrieve g from *irradiance* observations, using disort, and then we use this same disort to calculate DARE, HG(g) *represents* the phase function sufficiently well for our purposes. As you know, the first moment of the phase function along with a parametric HG phase function is sufficient to calculate fluxes with a two-stream approximation, whereas higher moments are required when using higher-stream RT (including disort). The higher moments of the phase function can be generated from g (higher powers of it; for example, the second moment is simply g^2). The retrieval uncertainty in g (provided in the manuscript) could be propagated into higher moments, but since they are derived from g for HG, this is not necessary here.

For the aerosol retrievals and DARE RT calculations, we simply set the "surface" to the level of the cloud and define the albedo as the spectral cloud albedo. Therefore, we do not model the surface in the main calculations within the manuscript. However, for the DARE parameterization, the spectral cloud albedo "grid" at each SZA was obtained through cloud optical thickness and effective radius retrievals.

The translation from the mid-visible albedo to the spectral albedo (described in Appendix A.3.2) starts with the originally measured albedo spectrum. From that, COD and REF are retrieved, from which the spectrum is calculated. For the other albedos in the "grid", the COD

is simply varied such that the albedo at the mid-visible wavelength changes as needed (while changing all of the other wavelengths as well).The COT/REF retrieval uses two wavelengths (860 and 1630 nm) to construct the lookup table, with no aerosol since the retrieval is done on the below aerosol, above cloud measurements. In these calculations, the surface for the cloud retrievals is standard Lambertian with an albedo value of 0.03. The COT range begins at 0, and this translates to a 0 "surface" albedo for the parameterization.

To address this comment in the manuscript, we added the following information to this section in the paper:

Lines 252/253: The RTM is run with 6 streams, assumes a Henyey Greenstein Phase function, and no delta-Eddington scaling is applied, all of which contribute to the inherent uncertainty within the RTM (Boucher et al., 1999).

Line 262: the RTM ingests the spectral cloud top albedo from SSFR (set as the surface within the model at the measured altitude, around 2km)

We should add that these simplifications were made to combine as many legs (cases) as possible in a common framework. In terms of radiative transfer, an opaque cloud effectively replaces the surface as boundary condition. However, for partially transparent clouds, the surface contributes to the reflectance. On the other hand, DARE is the *difference* between the fluxes with/without the aerosol above the altitude at which the albedo is prescribed in the model, and the approximations we used should therefore be insignificant compared to other uncertainties. Finally, it is acknowledged that clouds do not exhibit a Lambertian albedo. However, for irradiance calculations, the cloud albedo (non-Lambertian) can be substituted with a Lambertian albedo. A brief clarification on these subtleties has been included in the revised manuscript in Appendix section A.3.2, line 859-866.

Point 3: The authors chose a SZA of 20degrees to demonstrate the RT calculations and the parameterization fits. As demonstration purposes, this is OK, but there should be an acknowledgement that, when comparing to models, the DRE is typically calculated over the full range of SZAs that are experienced in the region and then diurnally averaged.

Thank you for bringing this up. To make it clear that our parameterizations are instantaneous, the sentence preceding eq 3 and eq 4 has been changed from "ORACLES measurements are used collectively to develop two parameterizations in the form of:" to "ORACLES measurements are used collectively to develop two parameterizations of instantaneous DARE in the form of:" In addition, we added the caveat to the caption figure 5: "It should be noted that a 20° SZA is not representative of the mean in the region." We have further added (lines 522-528) that in the first application of our parameterization, the diurnal integration will be done (see also our response regarding applications below).

Minor typos/clarifications

L24: spanned -> determined

The abstract has been rewritten (below, in blue) to better reflect the main goals of the paper. This wording no longer remains.

Revised Abstract: In this manuscript, we use observations from the NASA ORACLES (ObseRvations of CLouds above Aerosols and their intEractionS) aircraft campaign to develop a framework by way of two parameterizations that establishes regionally representative relationships between aerosol-cloud properties and their radiative effects. These relationships rely on new spectral aerosol property retrievals of the single scattering albedo (SSA) and asymmetry parameter (ASY). The retrievals capture the natural variability of the study region as sampled, and both were found to be fairly narrowly constrained (SSA: 0.83 ± 0.03 in the mid-visible, 532 nm; ASY: 0.54 ± 0.06 at 532 nm). The spectral retrievals are well suited to calculate the direct aerosol radiative effect (DARE) since SSA and ASY are tied directly to the irradiance measured in presence of aerosols – one of the inputs to the spectral DARE.

The framework allows for entire campaigns to be generalized into a set of parameterizations. For a range of solar zenith angles, it links the broadband DARE to the mid-visible aerosol optical thickness (AOD) and the albedo α of the underlying scene (either clouds or clear sky) by way of the first parameterization: P(AOD, α). For ORACLES, the majority of the case-to-case variability of the broadband DARE is attributable to the dependence on the two driving parameters of P(AOD, α). A second, extended, parameterization PX(AOD, α, SSA) explains even more of the case-to-case variability by introducing the mid-visible SSA ϖ as third parameter. These parameterizations establish a direct link from two or three mid-visible (narrowband) parameters to the broadband DARE, implicitly accounting for the underlying spectral dependencies of its drivers. They circumvent some of the assumptions when calculating DARE from satellite products, or in a modeling context. For example, the DARE dependence on aerosol microphysical properties is not explicit in P or PX because the asymmetry parameter varies too little from case to case to translate into appreciable DARE variability. While these particular DARE parameterizations only represent the ORACLES data, they raise the prospect of generalizing the framework to other regions.

L38: just off -> off (as the Sc extends 1000km....)

This has been adjusted.

L48-49: "In a region like the southeast Atlantic, this makes determining DARE challenging since the cloud fields change rapidly". I would suggest adding some idea of why the cloud changes rapidly - not only because of cloud dynamics, but because the cloud field advection is dominated by the flow in the MBL while the aerosol advection is dominated by the flow in the residual continental marine boundary layer which is frequently in the opposite direction.

Thank you, additional details have been included here (line 53)

L52: Chand was not the first to coin the phrase critical surface albedo. I'd suggest adding Haywood and Shine, 1995 reference here (Haywood, J.M., and Shine, K.P., 1995. The effect of anthropogenic sulfate and soot aerosol on the clear sky planetary radiation budget. Geophys. Res. Letts., 22, 5, 603- 606; see their Fig 1).

Reference has been added. Thank you for pointing out our oversight.

L75 (and probably other instances) aerosol optical depth -> AOD as you've already defined it

All instances have been updated.

I like Figure 1. It captures the essence of the filters and the criteria.

Thank you.

L148: Figure 3a -> Figure 2a.

Figure reference has been updated.

Caption for Figure 2. "c) The ratio between the BOL and TOL albedo spectra shown against the BOL AOD spectrum." I think that this needs a little more explanation. Presumably the AOD is 532nm? What about the albedo – is this the broadband albedo (i.e. weighted by the solar flux)?

Figure 2c shows the ratio between the two albedo spectra from 2b (BOL and TOL SSFR spectral albedo) as a function of the 4STAR AOD spectrum at the BOL. To make this more clear, the figure caption has been updated to: "c) The ratio between the BOL and TOL albedo spectra (taken from Fig 2b) shown against the BOL AOD spectrum at the 4STAR wavelengths. The intercept of the fit line is criteria 3 (AR_∞); if the intercept deviates largely from 1.0, the case cannot be used for an aerosol retrieval. Select wavelengths are labelled to highlight the spectral importance of this method."

In addition, the figure has been updated to highlight a few wavelengths so it is clear that the data shown is spectral. Below is the revised figure:

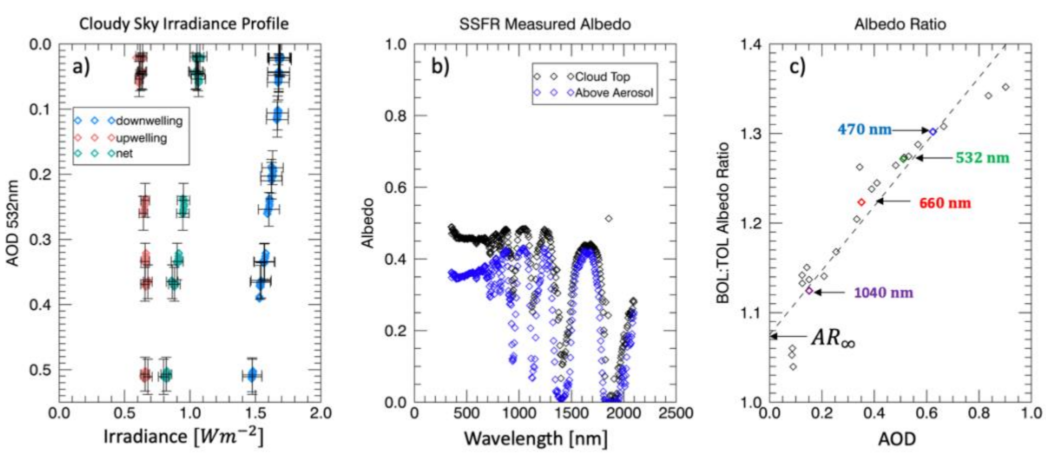

L163-L164: "The filter, which is applied to the upwelling profile, retains only those data within the 68% confidence interval (1 sigma) of the linear fit line". This is fine if the error distribution is Gaussian, but is it? It would be worth checking that this is the case. It seems as though the two cases where the original filtering method is retained may not be Gaussian which might give you a reason for applying a different filtering method.

Technically, the measurement data should be Gaussian, since Gaussian is essentially measurement repeatability with some variability. For the stationary condition, if we are measuring over the same surface the measurements should be Gaussian distributed, or if noise is present, that should be Gaussian distributed. However, if the cloud changes within the measurement period, one no longer measures the same thing, and that will be reflected in the data. The idea is that through the filtering, we get rid of anything that falls outside of that Gaussian envelope since the data become too unlikely.

In the original filtering method (from Cochrane et al., 2019), the 1-sigma standard deviation limit is based on the mean value of the profile. The updated filtering method uses the 1-sigma standard deviation based on the *linear fit* of the profile. In most cases, the new filtering provided better outcomes for the quality criteria (C1, C2, C3 in Fig 1) that follow the filtering, indicating that the new filter was eliminating more of the outlying data and retaining the quality data. However, in the exception cases, we found the opposite, and the new filter resulted in poorer values of the quality criteria. In these cases, we reverted back to the old filter method.

Below are the comparisons between the new and old filtering below (shown for the two exception cases that pass the criteria for a retrieval and one for a standard case that uses the new filtering). The cyan color is data within the 1 sigma fit and therefore retained; the lighter colors (pink, orange, purple) are data that do not pass the filter and not retained. In the first case, the new filter eliminates the highest AOD data. In the second case, the new filter retains too much variability at the highest AOD (lowest altitude).

Case 1:

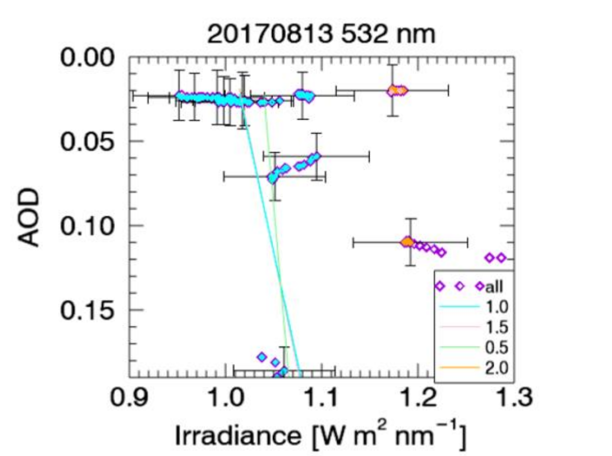

Original fit

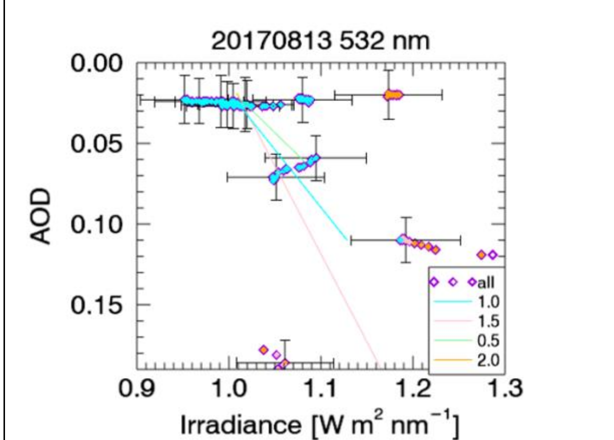

New fit

Case 2:

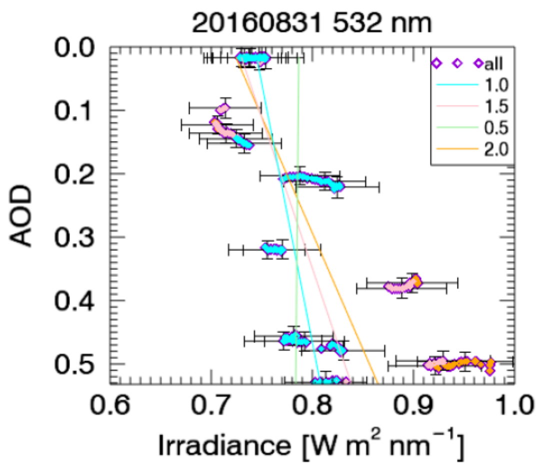

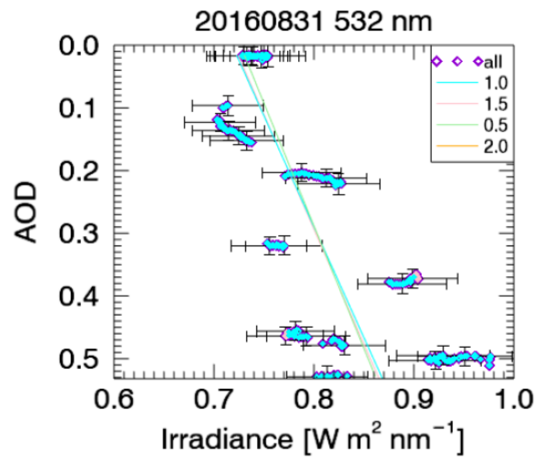

Original fit	**New fit**

In most cases, the difference between the two filtering methods is very small. Below is an example of a standard case for which the new fit is used.

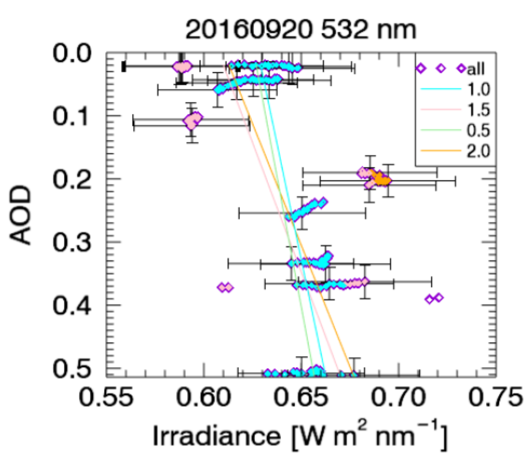

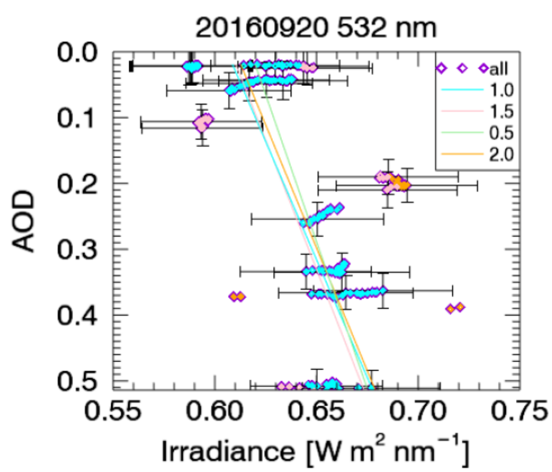

Original fit	**New fit**

Line 255. I was initially concerned that the retrieval algorithms rely on a mean solar zenith angle. The spirals typically take 30mins to achieve. This means that the SZA could be 15minutes out at the TOL and BOL. I reckon that 15minutes is approximately equivalent to 3.75degrees error is SZA given that the sza changes by around 15degrees per hour. So assuming a mean SZA of 30degrees (Table 2) could give an error of around 4% in the fluxes, or around 40Wm-2 assuming that you'd get around 1000Wm- 2 from the product of the solar constant and atmospheric transmission. However, I note from an earlier section (line 152) that the fluxes are

corrected according to Equation 3 of Cochrane et al. (2019); which is quite easy to miss on a first read. This therefore really needs to be reiterated here so emphasize that the observations are corrected and the observations and the modelling are therefore consistent.

Thank you – we have amended this to: "As mentioned in section 2.2.1, the irradiances are corrected to the SZA at the midpoint of the spiral to account for the changing solar position during the spiral. For consistency, the SZA within the RTM is set to the same SZA of the spiral midpoint." (lines 271-273)

L269: "We focus on the TOL calculations since radiative effects can be directly related to radiative balance at the TOL (Matus et al., 2015)." I think that it's better to say that the TOL calculations will resemble those calculated at the tropopause which is used as a metric for the cooling/warming impact of aerosols (e.g. Forster et al., 2007 which you already reference).

Thank you for pointing this out. Indeed, our TOL results should certainly resemble the top of the troposphere more than the entire column. Lines 285/286 have been updated accordingly.

L281: is DARE -> is the DARE

This has been updated (line 297).

L286: Russel -> Russell; deGraaf -> de Graaf

Thank you for catching this error, it has been corrected.

L288: "no studies that we are aware of have generalized RFE to account for these complexities in a quantitative framework." Be careful here. General circulation modelling studies can (and do) turn out these numbers on a regular basis simply by taking the all sky DARE and dividing it by the AOD, which implicitly has all of the detailed RT calculations implicit within it. It is quoted numerous times for different aerosol types for a multitude of e.g. AEROCOM simulations. You could also argue that above cloud satellite retrieval estimates have also implicitly accounted for this in their look-up-tables (e.g. de Graaf et al., 2012, which you already cite). What you mean is that "no detailed observational based studies"......

Based on your comment, it is clear that our intended meaning is not expressed through this statement and we therefore have decided to remove it from the manuscript. Rather than the RFE itself, this statement was intended to pertain to the parameterization, going from a single-parameter concept (RFE, used with AOD) to multiple parameters (as the ones driving P/PX, i.e., AOD, albedo, SSA).

L295: Again, some care is needed here: "has the significant advantage that the complexities of transitioning from narrowband to broadband for many parameters are incorporated into the parameterization coefficients, allowing for use across large spatial scales since minimal information is required". If you have a different type of aerosol, or your aerosol is mixed with mineral dust (as it frequently is in west Africa), then your algorithm will fail because the above cloud AOD and the DARE will differ when compared to BBA alone. This note of caution needs to be included I think – easiest way is to tone down the "large" spatial scales, which is semi-quantitative to "regional".

We agree that caution is needed in the application of the parameterization to larger regions, since with a different aerosol type the coefficients will no longer be valid. We have made this more clear by changing the text on lines 309-313 to: "has the significant advantage that the complexities of transitioning from narrowband to broadband for many parameters are incorporated into the parameterization coefficients, allowing for use across regional spatial scales for biomass burning aerosol since minimal information is required as input. Of course, the parameterization is only applicable for the region where the measurements were taken. It also cannot be generalized to apply for a different aerosol type."

L330: Russel -> Russell

This has been updated.

L356: Might want to include reference to the Wu et al. (2020) paper here as that suggests that there is a variation in the vertical profile of SSA.

Reference has been added to line 372/373, thank you.

L360: (scene or cloud albedo). I'm a little confused – is the scene albedo, the albedo with the aerosol and the cloud in it, while the cloud albedo is the albedo of the cloud layer alone? The two must differ otherwise the aerosol is having no effect. A few words of clarification would be appropriate.

When referring to scene albedo, we mean that as the scene *below* the aerosol layer. This work, especially in relation to the parameterizations, does not focus on the albedo measured from above the aerosol layer. For more clarity, line 92 in the paper has been changed from "The 550 nm albedo is the albedo of the scene below the aerosol layer and the SSA is a measure of aerosol absorption." to "The 550 nm albedo is the albedo of the scene below the aerosol layer (open ocean and/or cloudy scene), and the SSA is a measure of aerosol absorption."

We differentiate between scene and cloud in this instance because the parameterizations include albedo values down to 0. See also our response above how cloud-free scenes are handled in the radiative transfer.

L382 and Figure 5. The authors have tended to slip into the terminology of "surface albedo" which tends to mean the physical reflectance of the surface rather than the "effective underlying albedo" (i.e. the albedo of the combined Rayleigh scattering, cloud, MBL aerosol and surface) which is I think what the authors mean. Again, this should be clarified. Is there an explicit assumption that the underlying albedo is Lambertian? While this might be a decent approximation for heterogeneous thick cloud, is it sufficient for the sea-surface reflectance? What impact would this have?

There are several figures where the albedo goes down to zero, but Figure 10 suggested a minimum surface albedo of around 3.5%, which is similar to a 'real' ocean surface – some more explanation is warranted I think.

This is a very good point. All mentions of surface albedo in the manuscript have been changed to underlying albedo.

All of the albedo spectra in the paper are at cloud level, around 2 km, so they do include Rayleigh scattering. We realize Rayleigh scattering will change with altitude, but within the parameterization that change will be small (since the altitude variation between cases is small) and only would matter for the albedo translation. Within the radiative transfer calculations (as described under response to main point #2), the 'clear sky' 0 albedo is the albedo in the limit of 0 cloud optical thickness, and not a true clear sky with a 0 surface albedo.

Also, it is acknowledged that a sea surface is even less of a Lambertian reflector than a cloud (one only needs to think of sun glint). However, this is precisely the simplification that we made to fit both cloudy and cloud-free skies into a common framework. In a sense, one could call our albedo an "effective" albedo, which represents the true surface reflectance assuming a Lambertian reflectance distribution.

Finally, since we are looking at DARE (the difference of fluxes) rather than the fluxes themselves, our simplifications should lead to only negligible effects relative to the contributing measurement uncertainties. We have added details of this point in the manuscript in Appendix A.3.2, lines 859-866.

L385-386. Fig 7 is referred to before Figure 6. Easy to sort out by swapping the order of this sentence.

The sentence order has been switched (lines 409-411).

L405: "and rather strongly on the SZA (not shown; for example, it can attain 0.6 at low Sun elevations)." I think it would be appropriate to include a reference here – the classical reference for the dependence of the DRE on the radiative forcing is Boucher et al (1999) although this is for sulfate aerosol.

Thank you, reference has been added (line 429).

One of the problems with presenting the critical SSA for a solar zenith angle of 20degrees is this rather strong solar zenith angle dependence. The values at 20degrees (close to local noon) is not likely to be representative of the mean SZA that is experienced in the region. A caveat to in this regard would be appropriate.

Thank you, this caveat has been added into the caption of figure 5 (since this is the first figure shown at 20 degree SZA.) For your reference, below are the critical SSA figures for SZA=20 and SZA=40:

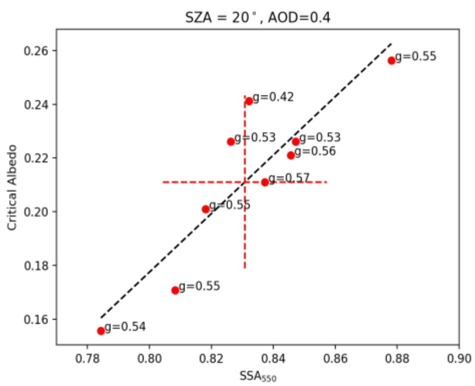

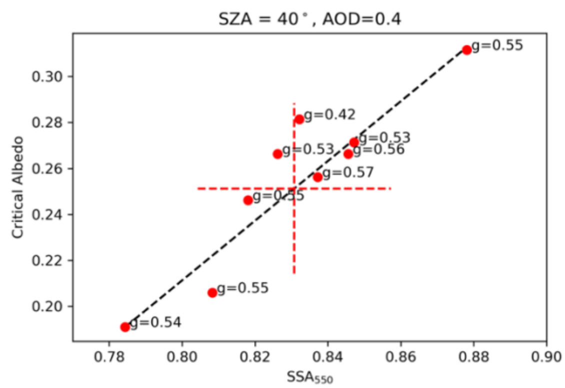

L 490: “We cannot judge whether our approach will be useful for predictive models, ... “. I agree that there are issues with whether the community will take up the parameterized approaches the RT calculations are a fundamental necessity. You might want to more explicitly suggest that a combination of lidar derived AODs and scene albedos from e.g. the geostationary GERB instrument or similar for future assessments of biomass burning DRE.

Thank you for this suggestion. In fact, we are working on an application paper that does just what you are suggesting here! We have included the additional statement on lines 520-525: “A promising approach in this regard is to use geostationary satellite retrievals of cloud and aerosol properties (Peers et al., 2020) in conjunction with in-situ aircraft data and radiative transfer calculations. Alternatively, one can use the satellite radiances to extrapolate from the spatially and temporally limited aircraft observations to obtain regional estimates of the diurnally-integrated DARE, circumventing the satellite retrievals. This approach, already underway within our group, builds on the *P* or PX parameterization, specifically by using albedo data from the geostationary Spinning Enhanced Visible and Infrared Imager (SEVIRI) in combination with ORACLES AOD data from HSRL-2 and 4STAR (Chen et al., 2020 in preparation). A grid-box specific model-to-observation inter-comparison is also underway in the wider ORACLES team. “

L494: “At the very least, the SSA and asymmetry parameter retrievals coming out of our and other ORACLES studies will constrain the aerosol optical properties in a range of models”. Again I agree – the text and references that document the very encouraging agreement between the absolute values of the SSA and the spectral dependence of the SSA and those from higher accuracy CRD and PAS measurement systems coming out of CLARIFY-2017 should again be noted here I think. I would also suggest changing “ORACLES studies” to “ORACLES/LASIC/CLARIFY-2017/AEROCLO-Sa studies (Zuidema et al., 2016)”.

We agree that this should be highlighted. The text has been updated to: “At the very least, the agreement between the absolute values and spectral dependence of the SSA and asymmetry parameter retrievals coming out of our and other ORACLES/LASIC/CLARIFY-2017/AEROCLO-Sa studies (Zuidema et al., 2016) such as Davies et al. (2019) and Wu et al. (2020) will provide robust and consistent constraints of the aerosol optical properties in a range of models.” (line 514-516)

List of relevant changes:

- **P.1-2, L. 21-39 (revised abstract)**
- **P.2, L. 53/54, 58**
- **P.3, L. 85, 92**
- **P.8, L. 252/253**
- **P.9, L. 262-263**
- **P.9, L. 271-173**
- **P.9, L. 285-286**
- **P.10, L. 297**
- **P.10, L. 309-313**
- **P.12, L. 372-381**
- **P.13, L. 409-411**
- **P.15-16, L. 514-516**
- **P.16, L. 520-526**
- **Figure 2 and caption**
- **Figure 5 caption**
- **Appendix A.3.2; P. 344-35, L. 859-866**

In addition to edits made according to the review comments, we have made the following updates:

- **Added uncertainty estimates to table 4b.**
- **Updated the SSA extrapolation and description (figure A1a), requiring the RT calculations be re-calculated.**
- **Updated Figures 5/9/10/11/D1/D2 and tables 4a and4b to reflect the new calculations**
- **Included supplementary material of code and coefficient files**

Dear reviewer,

Thank you for your thoughtful and constructive review of the manuscript. In the following paragraphs, we have summarized and responded to what we understand to be the main points of concern. We have also provided specific responses including plots to the individual minor comments.

Note: the color coding for the edit markings in the document are as follows:
Blue: directly addresses a comment from Reviewer #1
Green: directly addresses a comment from Reviewer #2
Red: additional update made by Authors

General comments/approach

It is evident from your comments that we are lacking clarity in the motivation of developing a DARE parameterization, which is key to the success of the paper. We appreciate this comment and acknowledge that the purpose was not made clear throughout the manuscript. The major advantage of developing the DARE parameterization is to encapsulate the transition from narrowband to broadband such that spectral aerosol and cloud properties are not required. The parameterizations require only one wavelength of input parameters and provides output of broadband DARE. Our goal was not to create an alternative to well-established radiative transfer formulae such as those presented in Coakley 1975, nor to replace full RT models such as libRadtran (with its solver "disort" created by Warren Wiscombe) [See our changes/additions on lines 99-101]. Rather, the difficulty concerns the *spectral* aerosol and cloud properties and their relationship to the *broadband* DARE. One cannot simply translate SSA, g, cloud albedo, etc. at a single wavelength into broadband DARE since their spectral dependencies are almost as important as the narrow-band single-wavelength values. Established formulae that are grounded in the physics (such as Coakley's or other 2-stream approximations) still require spectral properties and subsequent broadband integration. Here, we replace the need for a full spectrum with narrow-band quantities at a wavelength in the mid-visible wavelength range where they are often available, and we also side-step the spectral integration. This, rather than the radiative transfer itself, is the essence of this work. More generally, we cast the collective radiative observations into an ORACLES-wide set of formulae and "resolve" the case-to-case DARE variability in terms of only two (or three) driving parameters. To express this better, we re-wrote the abstract of the paper (included in blue font below), and made changes in other places of the manuscript (e.g., lines 99-101).

Revised Abstract: In this manuscript, we use observations from the NASA ORACLES (ObseRvations of CLouds above Aerosols and their intEractionS) aircraft campaign to develop a framework by way of two parameterizations that establishes regionally representative relationships between aerosol-cloud properties and their radiative effects. These relationships rely on new spectral aerosol property retrievals of the single scattering albedo (SSA) and asymmetry parameter (ASY). The retrievals capture the natural variability of the study region as sampled, and both were found to be fairly narrowly constrained (SSA: 0.83 ± 0.03 in the mid-visible, 532 nm; ASY: 0.54 ± 0.06 at 532 nm). The spectral retrievals are well suited to calculate the direct aerosol radiative effect (DARE) since SSA and ASY are tied directly to the irradiance measured in presence of aerosols – one of the inputs to the spectral DARE.

The framework allows for entire campaigns to be generalized into a set of parameterizations. For a range of solar zenith angles, it links the broadband DARE to the mid-visible aerosol optical thickness (AOD) and the albedo α of the underlying scene (either clouds or clear sky) by way of the first parameterization: P(AOD, α). For ORACLES, the majority of the case-to-case variability of the broadband DARE is attributable to the dependence on the two driving parameters of P(AOD, α). A second, extended, parameterization PX(AOD, α, SSA) explains even more of the case-to-case variability by introducing the mid-visible SSA ϖ as third parameter. These parameterizations establish a direct link from two or three mid-visible (narrowband) parameters to the broadband DARE, implicitly accounting for the underlying spectral dependencies of its drivers. They circumvent some of the assumptions when calculating DARE from satellite products, or in a modeling context. For example, the DARE dependence on aerosol microphysical properties is not explicit in P or PX because the asymmetry parameter varies too little from case to case to translate into appreciable DARE variability. While these particular DARE parameterizations only represent the ORACLES data, they raise the prospect of generalizing the framework to other regions.

The *application* of the parameterizations has been made clearer in the revised manuscript, with the important addition of explicitly stating how this is already being used to obtain diurnally-integrated values of DARE for the study region (lines 514-519). We are actively working on a publication that uses the parameterization to establish diurnally-integrated DARE for the study region, based on satellite observations and aircraft observations of AOD and albedo. It is important to note, however, that the parameterizations were not developed for regions *beyond* that of ORACLES, since as you pointed out, the physics in other regions are most likely different and ours is an empirical formula that applies only to the data it is based on (we alluded to aerosol microphysics specifically in the revised abstract quoted above). While we recognize that the number of cases is small, the range of properties they cover is likely sufficiently representative of the conditions in the study region for developing the parameterization scheme. As more cases become available, even those falling outside of the envelope of, say, previously observed single scattering albedo, the *relationship between* mid-visible aerosol properties (AOD, SSA, asymmetry parameter), albedo on the one hand, and broadband DARE on the other would likely be similar as well. The advantage of our framework is that it can be continually updated. This will be done, for example, with the aforementioned paper that we are currently working on. Whereas the present paper only considers ORACLES 2016 and 2017, the follow-up paper extends the parameterization to ORACLES 2018, prior to the application of the parameterization to the calculation of campaign-averaged DARE. Data from other campaigns (e.g., from CLARIFY or even SAFARI) could similarly be included.

We understand that the two parts of the paper seem distinct from one another, and this is done purposefully. The manuscript is the second part to its companion paper, Cochrane et al., 2019, and they are meant to be read in succession. However, it was important that we include enough detail in the first part of the paper on the retrieval algorithm such that it can be understood at a surface level without reading the 2019 companion paper, as well as to make clear the changes made to the algorithm relative to the version described in the 2019 paper. The most important change of the 2020 version of the algorithm relative to its 2019 predecessor is that the data are automatically filtered and conditioned in a consistent manner. This allows ingesting of data without different treatment of cases and thereby biasing the results. In addition, part I of the current paper provides a data product on its own: the aerosol property retrievals of SSA and g. This database of these retrievals, though small, is important to include along with the parameterization of DARE as presented in part II.

To address your concerns, here is what we have done within the revised manuscript:

First, the abstract has been revised to better reflect the overall goals of the paper (see draft above in blue). Second, the two parts of the paper are now delineated at the end of the introduction (Lines 115-119). Regarding the body of the paper: The original version did not effectively capture the main objectives of the paper and potentially left the reader with an incorrect impression of what the paper is about. In the revised version, the benefit of a direct transition from narrowband to broadband through our parameterization has been highlighted in greater detail (lines 309-314). In addition, the application of our parameterizations has been more explicitly described (using the next paper as example; lines 514-519). We have made the separation between part I and part II of the paper even more apparent, making it possible to skip the aerosol property retrieval section and move directly into the DARE section (lines 115-119; section headings). However, we are hesitant to significantly reduce this section because of its value to the southeast Atlantic region research community.

Thank you again for your review of the paper and we hope that our changes have addressed your concerns satisfactorily.

With the above comments, we believe that we addressed the general (major) comments. Our response to sequential (minor) comments is below (in blue).

Minor comments:

Line 24: Does the "scene albedo" actually mean cloud albedo? If it really means "scene albedo" then what types of scenes (ocean, land, snow etc.) have been included?

ORACLES data was exclusively taken over the southeast Atlantic ocean. We use "scene albedo" rather than "cloud albedo" since we encountered scenes that included both cloudy and clear sky (partially cloudy or area contained cloud holes.) This is clarified in the revised manuscript at line 92 (and described in the newly drafted abstract quoted above).

Line 86: similarly, it should be clarified here if "scene albedo" actually just means "cloud albedo". Note that the spectral signature of land reflectance/albedo is very different from cloud albedo.

Thank you for pointing out this ambiguity. For more clarity, line 92 has been changed from "The 550 nm albedo is the albedo of the scene below the aerosol layer and the SSA is a measure of aerosol absorption." to "The 550 nm albedo is the albedo of the scene below the aerosol layer (open ocean and/or cloudy scene), and the SSA is a measure of aerosol absorption." A detailed discussion of the albedo has also been included in Appendix A.3.2.

Eq. (3) and (4): It should be pointed out explicitly if these equations are for instantaneous or diurnal averaged DARE. Also why is the dependence of DARE on solar zenith angle omitted in these equations? SZA is part of the parameterization (Table 4b), no?

Thank you, the sentence preceding eq 3 and eq 4 (line 85) has been changed from "ORACLES measurements are used collectively to develop two parameterizations in the form of:" to "ORACLES measurements are used collectively to develop two parameterizations of instantaneous DARE in the form of:"

The dependence of DARE on SZA is not included in these equations, since the parameterization coefficients themselves do not depend on SZA. Rather, the parameterization coefficients are calculated separately for a range of SZAs.

To what extent is the DARE dependent on atmospheric profiles, such as water vapor profiles? There are some recent studies that suggest a correlation between the presence of above-cloud smoke and an enhanced water vapor in the ORACLE region. Should this correlation be considered in the parameterization?

This is an important question. The dependence of DARE on atmospheric profiles, specifically water vapor, is implicitly included within the parameterization. Each case that the parameterization is based upon has the measured water vapor profile included in its DARE calculations.

While we do not determine the extent to which DARE depends on water vapor, it should not depend too much on it since DARE is defined as Fnet (with aerosol) – Fnet (without aerosol). The water vapor profile for both terms was held fixed (as determined from observations for each of the cases), and therefore only has a bearing on DARE if it affects the incident radiation on top of the aerosol layer. Compared to the impact of the scene AOD, albedo, and SSA on the case-to-case DARE variability, the water vapor profile variability (as well as the aerosol microphysics variability) was negligible. However, the water vapor does have a bearing on the total heating rates, which is explored in a separate paper (in progress; if submitted before this paper is accepted, we will include a reference in the appropriate place)

Cochrane et al., 2019.has been cited many times in the paper, often in different formats. Please be consistent and also considering use abbreviation e.g., C19 to refer to Cochrane et al., 2019.

Thank you for catching this. The references to Cochrane et al., 2019 have been abbreviated to C19 (defined upon its first occurrence).

Line 148: Figure 3 should be Figure 2.

Thank you. This has been updated in line 156.

Eq. (5) and (6), why are the parameters a_lambda and b_lambda the same for upward and downward irradiances? What is the underlying physics?

Thank you for pointing this out, as our notation is ambiguous. $a_\lambda^\uparrow$ is not the same as $a_\lambda^\downarrow$ (similar for $b_\lambda^\uparrow$ and $b_\lambda^\downarrow$; equation 6 has been changed to $c_\lambda^\uparrow$ and $d_\lambda^\downarrow$ (line 171).

Again, Section 2.2.1 and 2.2.2 seem to be a replay of Cochrane et al., 2019. They should be put in the Appendix or substantially shortened.

As noted in the response to the general comments, we understand that the two parts of the paper seem distinct from one another, and this is done purposefully. The manuscript is the second part to its companion paper, Cochrane et al., 2019, and they are meant to be read in succession. However, it is important that we include enough detail in the first part of the paper on the retrieval algorithm such that it can be understood at a surface level without reading the 2019 companion paper, as well as to make clear the changes made to the algorithm relative to the version described in the 2019 paper. The most important change of the 2020 version of the algorithm relative to its 2019 predecessor is that the data are automatically filtered and conditioned in a consistent manner. This allows ingesting of data without different treatment of cases and thereby biasing the results. In addition, part I of the current paper provides a data product on its own: the aerosol property retrievals of SSA and g. This database of these retrievals, though small, is important to include along with the parameterization of DARE as presented in part II.

To address your concern, we have added additional text on lines 115-119 to better describe the two parts of the paper and have updated the section headings to reflect the separation (line 326).

Around line 150, this part is confusing and needs detail explanation. For example, “both upwelling (F_up) and downwelling (F_dn) irradiance profiles have an approximately linear relationship to AOD due to the absorption and scattering of the aerosol layer.” Shouldn’t the downwelling (F_dn) be exponential with AOD as a result of Beer’s law? “Any deviation from the linear relationship is attributed to changes in the underlying cloud” Why? Can’t the vertical variation of aerosol properties, e.g., SSA and/or g cause deviation from the linear relationship? How does cloud cause the deviation? These questions need to be clarified.

We did not intend to imply that the direct downwelling irradiance should not follow Beer’s law. However, in the SSFR measurements we cannot separate the global irradiance into its diffuse and direct components. We are using the linear assumption for the global downwelling as a simplification only for initial fitting for the subsequent filtering. We agree with the reviewer here because indeed, deviations from the linear relationship could be due to non-linearities as expected from Beer’s law, or vertical dependencies of aerosol parameters. However, we expect these to be negligible compared to changes in the underlying clouds, and therefore use deviations from a linear profile – just to filter our data. Otherwise, the results of the paper (i.e., the retrievals and the calculations) are not predicted on any linearity assumptions.

As can be seen from the figures below, the direct-beam downwelling (labeled SPN-f, SPN-S) *does* follow an exponential (these measurements were only available during 2018, and they are therefore not included in this manuscript). However, the global downwelling (SSFR global, green) can be approximated with a linear fit, at least for the range of AOD we encountered. We should add that the thin-layer approximation introduced by, e.g., Coakley et al. (1975) shows a linear dependence of the global reflectance analytically ("In the thin atmosphere approximation, the reflectivity and transmissivity of the layer are linear functions of its optical depth"). The figure below on the right shows the irradiance components as a function of altitude.

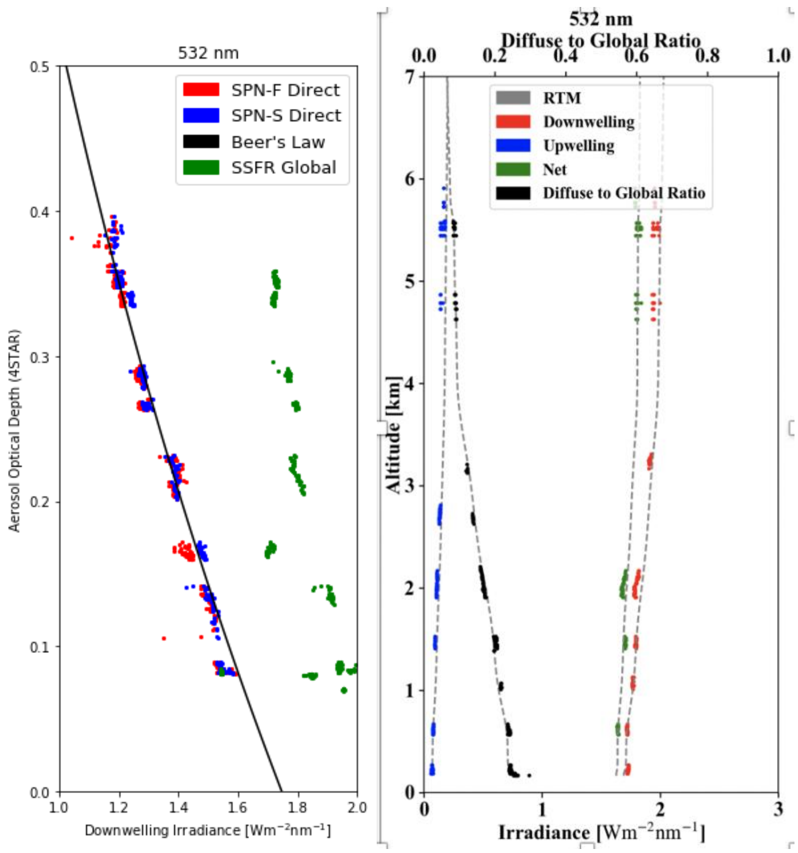

While vertical variation of the aerosol properties could theoretically affect the linear relationship that we assumed, but changes in the cloud properties below outweigh aerosol-induced deviations from a linear profile by far, and can therefore be used as the basis for filtering.

To address this comment, we have added the following additional text on lines 159-163:

"This linear assumption for the global downwelling is a simplification only for initial fitting for the subsequent filtering, and deviations from the linear relationship could be due to non-linearities as expected from Beer's law, or vertical dependencies of aerosol parameters. However, we expect these to be negligible compared to changes in the underlying clouds, and therefore use deviations from a linear profile to filter our data."

Does the retrieval algorithm assume H-G phase function? What are the higher-order terms of the phase function expansion other than asymmetry factor, g? What is the uncertainty associated with the phase function assumption?

Yes, it does assume an Henyey-Greenstein (HG) phase function with our retrieved asymmetry parameter (the first moment of the actual phase function) as input. The first moment of the phase function along with a parametric HG phase function is sufficient to calculate fluxes with a two-stream approximation. Higher moments are required when using higher-stream RT models (including disort) and can be generated from g (higher powers of it; for example, the second moment is simply g^2). We do not at all claim here that HG is, in fact, the actual phase function. On the contrary, the real phase function most likely deviates from HG. However, HG(g) *represents* the real phase function sufficiently well for our purposes. Using Coakley '75 again as an example: He does show that there are differences in the reflectance when using a two-stream formula relative to a multi-stream (in this case, doubling adding) RT. However, these differences arose because they were looking at directional reflectance. In our case, we retrieve g from *irradiance* observations, using disort, and then we use this same disort to calculate DARE. The retrieval uncertainty in g (provided in the manuscript) could propagate into higher moments, but since they are trivially derived from g for HG (g^2, g^3, etc.), this is not necessary here.

The following additional text is included at lines 253/254:

"The RTM is run with 6 streams, assumes a Henyey Greenstein Phase function, and no delta-Eddington scaling is applied, all of which contribute to the inherent uncertainty within the RTM (Boucher et al., 1999)."

Line 286: Russel et al., 1997 should be Russell et al., 1997; deGraaf should be de Graaf

Thank you for pointing out these errors. We have removed this statement and the associated references due to a comment from another reviewer.

Eq. (12) and (13): The formula looks quite arbitrary. Is there any physics behind these polynomial parametrizations or are they only empirical? Note that there are some well-established 2-stream or 4-stream formula for layer reflection, e.g., Coakley (1975). Is it possible to draw some theoretical basis or physical meaning for the parameterization from these 2-stream or 4-stream approximations? Also, some previous studies have tried to use the concept of adding doubling to approximate the reflection of two layers (Lenoble 1985). Do you think these formulae might be helpful?

Thank you for this comment. Please see our general response above, in addition to our subsequent response. While the 2-stream (or 4-stream) formulae are appropriate for many applications, they are not suited for what we capture with our parameterization (see also general comments at the beginning of this response). What we have developed in this manuscript is not about the approximation, or creating a new approximation, but to directly represent the relationship between narrowband to broadband for which the spectral dependencies are implicit. The approximation formulas presented in Coakley (1975) would not work for our application because they would still require *spectral* properties which would need to be averaged or parameterized first, which is not as direct as our parameterization.

In addition, the approximations are not sufficiently accurate for our purposes since simplifications are required in these analytical formulae. For example, the thin layer approximation by Coakley '75, eq 23 (which does take absorption into account, for non-black surfaces) starts deviating even for fairly small optical thickness as can be seen in the figure below. Additionally, the non-linearity of DARE as a function of AOD (known from RTM calculations) would not be represented by the thin layer approximation.

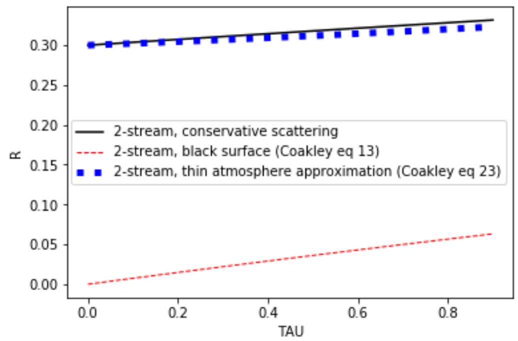

To address your comment, we have added the following additional text on lines 99-101: "They are not meant to replace detailed or approximated radiative transfer calculations (e.g., Coakley 1975), which would require all these inputs, but rather to arrive at a broadband DARE with a minimum set of input parameters that drive its regional variability."

Why is SZA dependence of DARE omitted in Eq. (12) and (13)?

The dependence of DARE on SZA is not included in these equations since the parameterization coefficients themselves do not depend on SZA. Rather, the parameterization coefficients are calculated separately for a range of SZAs.

Eq. (14) and (15): again, these parameterizations look arbitrary. Is there any underlying physics?

The underlying physics are only included insofar as that we parameterized broadband DARE as a functional dependence with respect to its driving parameters. The only way to transition from narrowband to broadband is through polynomial fitting; there is no direct way to include the physics of radiative transfer in aerosol layers above clouds, which has been well established since the mid-1970s. Of course, one could calculate the broadband DARE if all of the parameters were available, but that is not the point of this paper (see the other comments above). What we have developed in this manuscript is not about the approximation, or creating a new approximation, but to directly represent the relationship between narrowband to broadband for which the spectral dependencies are implicit. The analytical formulas which are based on physics do not work for our application because they would still require *spectral* properties which would need to be averaged or parameterized first, which is not as direct as our parameterization.

To make this more clear in the manuscript, additional text has been added on lines 99-101 and 309-314;

Eq. 21 – 24: I understand that dSSA term is introduced to make the parameterization scheme more general and more accurate. But as I mentioned above, a broadband RTM can easily compute the DARE given any type of SSA and g. Why bother developing such a complicated parameterization?

The parameterization removes the necessity of *spectral* SSA and g which are often difficult to obtain. We fully agree with the reviewer though: An RTM model would be more appropriate to compute the DARE *if* (!) spectral properties were known. However, most often spectral quantities are *not* known, unless they are tied to a fixed aerosol "type" that tabulates the spectral dependence (e.g., OPAC). More importantly, we show that *we do even not need to know these spectral detail*s as *explicit* inputs since just a few (2 or 3) mid-visible parameters explain the variability of DARE across the ORACLES cases we analyzed *to within the measurement uncertainty*. The spectral dependence of the parameters as measured/retrieved is thereby *implicitly* accounted for, and we can thus obtain broadband DARE with a minimum number of input parameters.

We have addressed this comment with revised abstract as well as the additional text on lines 99-101; 309-314; 522-528.

List of relevant changes:

- P.1-2, L. 21-39 (revised abstract)
- P.3, L. 91-92
- P.3, L. 99-101
- P.4, L. 110
- P.4, L. 115-119
- P.5, L. 157, 163, 164
- P.5, L. 158-162
- P.6, L. 170-173
- P.6, L. 177, 182
- P.7, L. 203, 211, 216
- P.8, L. 246
- P.8, L252-253
- P.9, L. 260
- P.10, L309-314
- P.11, L. 326
- P.17, L. 522-528

In addition to edits made according to the review comments, we have made the following updates:

- Added uncertainty estimates to table 4b.

- Updated the SSA extrapolation and description (figure A1a), requiring the RT calculations be re-calculated.
- Updated Figures 5/9/10/11/D1/D2 and tables 4a and 4b to reflect the new calculations
- Included supplementary material of code and coefficient files

Empirically-Derived Parameterizations of the Direct Aerosol Radiative Effect based on ORACLES Aircraft Observations

Sabrina P. Cochrane[1,2], K. Sebastian Schmidt[1,2], Hong Chen[1,2], Peter Pilewskie[1,2], Scott Kittelman[1], Jens Redemann[3], Samuel LeBlanc[4,5], Kristina Pistone[4,5], Meloë Kacenelenbogen[4], Michal Segal Rozenhaimer[4,5,6], Yohei Shinozuka[4,7], Connor Flynn[8], Amie Dobracki[9], Paquita Zuidema[9], Steven Howell[10], Steffen Freitag[10], Sarah Doherty[11]

[1]Department of Atmospheric and Oceanic Sciences, University of Colorado, Boulder, 80303, USA
[2]University of Colorado, Laboratory for Atmospheric and Space Physics, Boulder, 80303, USA
[3]School of Meteorology, University of Oklahoma, Norman, Oklahoma, 73019, USA
[4]NASA Ames Research Center, Mountain View, 94035, USA
[5]Bay Area Environmental Research Institute, Mountain View, 94035, USA
[6]Department of Geophysics and Planetary Sciences, Porter School of the Environment and Earth Sciences, Tel-Aviv University, Tel-Aviv, Israel
[7]Universities Space Research Association/NASA Ames Research Center, Mountain View, 94035, USA
[8]Pacific Northwest National Laboratory, Richland, Washington, 99354, USA
[9]Department of Atmospheric Science, Rosenstiel School of Marine and Atmospheric Science, University of Miami, Miami, FL, 33146, USA
[10]Department of Oceanography, University of Hawaii, Honolulu, HI, 96822, USA
[11]Joint Institute for the Study of Atmosphere and Ocean, University of Washington, Seattle, WA, 98195, USA

Correspondence to: Sabrina P. Cochrane (sabrina.cochrane@colorado.edu)

Abstract. In this manuscript, we use observations from the NASA ORACLES (ObseRvations of CLouds above Aerosols and their intEractionS) aircraft campaign to develop a framework by way of two parameterizations that establishes regionally representative relationships between aerosol-cloud properties and their radiative effects. These relationships rely on new spectral aerosol property retrievals of the single scattering albedo (SSA) and asymmetry parameter (ASY). The retrievals capture the natural variability of the study region as sampled, and both were found to be fairly narrowly constrained (SSA: 0.83 ± 0.03 in the mid-visible, 532 nm; ASY: 0.54 ± 0.06 at 532 nm). The spectral retrievals are well suited to calculate the direct aerosol radiative effect (DARE) since SSA and ASY are tied directly to the irradiance measured in presence of aerosols – one of the inputs to the spectral DARE.

The framework allows for entire campaigns to be generalized into a set of parameterizations. For a range of solar zenith angles, it links the broadband DARE to the mid-visible aerosol optical thickness (AOD) and the albedo (α) of the underlying scene (either clouds or clear sky) by way of the first parameterization: P(AOD, α). For ORACLES, the majority of the case-to-case variability of the broadband DARE is attributable to the dependence on the two driving parameters of P(AOD, α). A second, extended, parameterization PX(AOD, α, SSA) explains even more of the case-to-case variability by introducing the mid-visible SSA ϖ as third parameter. These parameterizations establish a direct link from two or three mid-visible (narrowband) parameters to the broadband DARE, implicitly accounting for the underlying spectral dependencies of its drivers. They circumvent some of the assumptions when calculating DARE from satellite products, or in a modeling context. For

example, the DARE dependence on aerosol microphysical properties is not explicit in P or PX because the asymmetry parameter varies too little from case to case to translate into appreciable DARE variability. While these particular DARE parameterizations only represent the ORACLES data, they raise the prospect of generalizing the framework to other regions.

1 Introduction

During the African burning season of August-October, a semi-permanent stratocumulus cloud deck off the southern African west coast is overlaid by a thick layer of biomass burning aerosols. These aerosols are advected over the southeast Atlantic Ocean from the interior of the African continent and account for nearly 1/3 of the total global biomass burning aerosol (van der Werf et al., 2010). The seasonal environment of high biomass aerosol loading above clouds has large, variable radiative impacts that have yet to be fully characterized.

In addition to many other science objectives, the NASA ORACLES aircraft campaign aimed to obtain the Direct Aerosol Radiative Effect (DARE) in both cloudy and clear skies for this region (Zuidema et al., 2016; Redemann et al., 2020). The distinction between DARE in cloudy versus clear skies is crucial since the albedo below an aerosol layer strongly influences the sign and magnitude of DARE. The albedo from below an aerosol layer can determine the sign of the top of the atmosphere (TOA) DARE independently of the aerosol itself (Twomey, 1977; Hansen et al., 1997; Russell et al., 2002; Keil and Haywood, 2003; Yu et al., 2006; Chand et al., 2009; Zhang et al., 2016; Meyer et al., 2013; Meyer et al., 2015). In a region like the southeast Atlantic, this makes determining DARE challenging since the cloud fields change rapidly according to the flow of the marine boundary layer. Depending on the cloud albedo, the aerosol could be warming (positive DARE) or cooling (negative DARE) at the TOA (Yu et al., 2006; Russell et al., 2002; Twomey, 1977). The albedo value where DARE transitions from positive to negative, or warming to cooling, is known as the critical albedo (Haywood and Shine, 1995; Russell et al., 2002; Chand et al., 2009).

The spectral DARE in $Wm^{-2}nm^{-1}$ is determined from the difference between the net irradiance (F_λ^{net}) with and without the aerosol layer:

$$DARE_\lambda = F_{\lambda,aer}^{net} - F_{\lambda,no\ aer}^{net}. \tag{1}$$

Aircraft measurements, such as those collected during ORACLES, provide direct observations of the components necessary to calculate DARE. However, measurements are only taken for a sub-sample in time and space and may not be representative of the region as a whole. DARE calculated from aircraft observations alone would therefore leave the larger question of whether the aerosols warm or cool the southeast Atlantic unanswered.

In the case of DARE, the translation from individual observations into a common framework was first introduced by Meywerk and Ramanathan (1999). The radiative forcing efficiency (RFE) empirically relates DARE to the aerosol optical depth (AOD):

DARE=RFE*AOD. (2)

The RFE is defined as the (usually broadband) DARE normalized by the (usually mid-visible) AOD, or sometimes as the derivative of DARE with respect to the AOD. It can be regarded as an intensive property of an airmass that allows the direct conversion from AOD to DARE, complementing calculations based on aerosol microphysical and optical properties. When the RFE is aggregated for an entire field mission, it can provide a representative airmass characteristic that lends aircraft observations a broader scientific impact than the contributing individual measurements. If aerosol microphysical and optical properties are insufficiently known in a region of interest, this mission-aggregated RFE constitutes a DARE parameterization that solely requires AOD (equation 2). If the RFE varies little in a region and season of interest, it can be used to derive regional DARE estimates via AOD statistics from satellites – at least in principle. More fundamentally, observations of the dependence of flux changes on AOD help to develop confidence in radiative forcing calculations based on measured aerosol properties (Russell et al., 1999, Redemann et al., 2006). In this sense, the RFE in conjunction with Eq. (2) provides closure to those calculations, and thus constrains them from the radiative flux and DARE perspective.

In this paper, we generalize the concept of RFE by explicitly taking into account the dependencies of DARE not only on AOD as expressed in equation (2), but also on both the aerosol and cloud properties. ORACLES measurements are used collectively to develop two parameterizations of instantaneous DARE in the form of:

$$DARE = P(AOD_{550\,nm},\ \alpha_{550\,nm}), \quad (3)$$

and

$$DARE = PX(AOD_{550\,nm}, \alpha_{550\,nm},\ SSA_{550\,nm}), \quad (4)$$

where AOD, α and SSA are the aerosol optical depth, albedo, and single scattering albedo at 550 nm. The 550 nm albedo is the albedo of the scene below the aerosol layer (open ocean and/or cloudy scene), and the SSA is a measure of aerosol absorption. *P* stands for the two-parameter representation of DARE and *PX* stands for an extended version with three parameters. Both parameterizations provide instantaneous *broadband* DARE that are based upon *spectral* aerosol and cloud properties. The right-hand sides of equations 3 and 4 are mid-visible quantities, while the left-hand sides are broadband results. The parameterizations have the advantage of implicitly accounting for the spectral dependencies of the aerosol and cloud properties (e.g. aerosol scattering phase function, aerosol vertical distribution, spectral dependence of aerosol absorption, cloud optical depth, cloud effective radius, cloud top and base height), whereas the dependence on mid-visible AOD, SSA, scene albedo, and solar zenith angles is explicit. They are not meant to replace detailed or approximated radiative transfer calculations (e.g., Coakley 1975), which would require all these inputs, but rather to arrive at a broadband DARE with a minimum set of input parameters that drive its regional variability.

From the user standpoint, applying the parameterizations is straightforward because broadband DARE can be estimated with minimal information on the cloud and aerosol properties. The parameterization coefficients encompass the many complexities of transitioning from narrowband to broadband, such that the spectral dependencies of the cloud and aerosol properties are not necessary. Of course, the parameterization only represents the "mean" conditions encountered in the ORACLES region and sampling time, and it becomes invalid outside of this mission envelope. Equation (3) only requires AOD and scene albedo at mid-visible 550 nm, which can be readily obtained from satellite observations. If mid-visible SSA is also known (from satellite or aircraft retrievals, in-situ observations, or from a climatology), the second parameterization (Eq. 4) can be used, which decreases the uncertainty of DARE, as we will discuss below.

To arrive at the final parameterizations, we first build upon the method presented in Cochrane et al. (2019; further denoted as C19) and determine the aerosol intensive properties of SSA and asymmetry parameter (*g*) that best represent the ORACLES region during August and September of 2016 and 2017. We evaluate the radiative effects of those aerosols where the relationships found between DARE, AOD, and albedo form the foundation of the parameterizations that capture the collective variability sampled from the viable cases from ORACLES 2016 and 2017.

The paper has two parts, which can be read independently depending on the reader's main interest: In the first part (Section 2), we describe the data and the methods used to determine spectrally resolved SSA and *g*. We generalize earlier work (C19) by adding a methodology for a uniform processing of multiple cases. The second part (Section 3) translates AOD, albedo, and SSA into DARE, and the *P* and *PX* parameterizations are constructed by progressively capturing more of the case-to-case DARE variability. In Section 5, we provide a quick summary and interpretation of both parts of the paper.

2 Data and Methods

2.1 Data

The ORACLES project conducted research flights in the southeast Atlantic for 3 one-month periods over three consecutive years (2016-2018) during the burning season to study the biomass burning aerosols and stratocumulus cloud deck. To achieve the defined science objectives, the ORACLES project made use of the NASA P-3 aircraft for the duration of the experiment and the NASA ER-2 aircraft in 2016 only. Between the 2016 and 2017 deployments, the P-3 completed 26 science flights, five of which were collocated with the ER-2. All data can be found on the NASA ESPO archive website (ORACLES Science Team, 2017a, b, 2019).

We focus on utilizing measurements taken from the P-3, primarily the irradiance measurements taken by the Solar Spectral Flux Radiometer (SSFR, Pilewskie et al., 2003; Schmidt and Pilewskie, 2012) in conjunction with AOD and retrievals of column gas properties from the Spectrometer for Sky-Scanning Sun-tracking Atmospheric Research (4STAR, Dunagan et al., 2013; Shinozuka et al., 2013; LeBlanc et al., 2020) to achieve the specific goals of this paper. SSFR consists of two pairs of spectrometers. Each pair (one zenith viewing and one nadir viewing) covers a wavelength range of 350-2100 nm. SSFR is radiometrically and angularly calibrated pre- and post- mission. Its zenith light collector is equipped with an active leveling platform (ALP), which keeps it horizontally aligned by counteracting the variable aircraft attitude. This allows the collection of irradiance data as long as pitch and roll stay within the ALP operating range of 6°. This ensures that radiation from the lower hemisphere does not contaminate the zenith irradiance measurements, which was especially important for the bright clouds encountered during ORACLES. 4STAR provides spectral retrievals of AOD from the solar direct beam irradiance above the aircraft and is calibrated through Langley extrapolation technique before and after deployment at Mauna Loa Observatory along with in-flight high-altitude measurements (see LeBlanc et al., 2020 for details on 4STAR calibration). 4STAR also provides aerosol intensive properties (e.g., SSA described in Pistone et al. 2019), column water vapor and trace gas retrievals, such as ozone (e.g., Segal-Rosenheimer et al., 2014). Further details on SSFR, ALP and 4STAR instrumentations and calibrations can be found in Cochrane et al. (2019).

2.2 Methods

To construct our DARE parameterizations, aerosol intensive optical properties such as SSA and *g* must be determined for as many cases as possible. Retrieving these properties from aircraft irradiance measurements is inherently challenging because the aerosol radiative effects can be relatively small compared to the horizontal variability of cloud albedo.

C19 showed for two cases that special spiral maneuvers ("square" spiral) are more successful than the heritage "stacked leg" approach because multiple measurements are taken throughout the vertical profile over a short time period (typically 20 minutes). This sampling strategy reduces the effects of cloud inhomogeneities and allows isolation of the aerosol signal, as long as specific quality criteria (detailed below) are met. These criteria, preceded by two filtering steps in which data points are removed, are described in the following section and follow the order presented in the flow chart of Figure 1. The filters and criteria provide objective data conditioning prior to the subsequent aerosol retrieval and DARE parameterizations.

2.2.1 Data Conditioning

Throughout the spiral, the zenith (downwelling) and nadir (upwelling) irradiance measurements are continuously affected by the aerosol layer. The aerosol-induced changes to the irradiance profiles allow us to extract information about the aerosol itself. As can be seen in Figure 2a, both upwelling ($F_\lambda^\uparrow$) and downwelling ($F_\lambda^\downarrow$) irradiance profiles have an approximately linear relationship to AOD due to the absorption and scattering of the aerosol layer. Any deviation from the linear relationship is attributed to changes in the underlying cloud; these are filtered out to isolate the radiative effect of the aerosol. This linear assumption for the global downwelling is a simplification only for initial fitting for the subsequent filtering, and deviations from the linear relationship could be due to non-linearities as expected from Beer's law, or vertical dependencies of aerosol parameters. However, we expect these to be negligible compared to changes in the underlying clouds, and therefore use deviations from a linear profile to filter our data.

Following the methods described in C19, two filters are applied to the data to ensure the isolation of aerosol effects. Prior to filtering, all data are corrected to the SZA at the midpoint of the spiral according to Equation 3 in C19 to account for the minor change in solar position throughout the spiral. The first is an altitude filter (see F1 in Fig. 1), where the altitude range is limited to encompass only the vertical extent of the aerosol layer. The second is a homogeneity filter (see F2 in Fig. 1), which selects the dominant profile of measurements, whether that be cloudy or clear sky, and removes any outlying data. The filter begins with a linear fit of the irradiances with respect to the AOD for each wavelength:

$$F_\lambda^\uparrow = a_\lambda^\uparrow + b_\lambda^\uparrow * AOD_\lambda, \quad (5)$$

$$F_\lambda^\downarrow = c_\lambda^\downarrow + d_\lambda^\downarrow * AOD_\lambda, \quad (6)$$

where a_λ and b_λ (c_λ and d_λ) are the slope and intercept of the linear regression, for which the individual data points are weighted inversely by the irradiance uncertainties. In any particular spiral, the measurements could be taken from either predominantly cloudy or clear sky. The filter, which is applied to the upwelling profile, retains only those data within the 68% confidence interval (1 sigma) of the linear fit line. This ensures that the retained data contains no outlying points and is all from one mode: clear sky or cloudy sky. This filtering step is slightly modified from the method presented in C19 in two ways: 1) the irradiances were previously fit against AOD at 532 nm only rather than AOD at the corresponding wavelength and 2) the range of retained data was previously based on the confidence interval of overall mean irradiance value rather than the confidence interval of the linear fit throughout the profile. We have made these adjustments to better allow for linear variation with altitude while eliminating data that significantly deviates from the profile. There are 3 exception cases for which we maintain the original filtering from C19 using the confidence interval on the mean value. For these cases, the filtering modification overly eliminated data or retained excessive variability at small (large) AOD values (high altitude (low altitude)).

Following the filters, each case must pass criteria that ensure the changes in net irradiance with altitude are caused by the aerosol radiative effects and not variability in the underlying cloud field. First, irradiance measurements must be available throughout the spiral, spanning the full AOD dynamic range between the top and bottom of the layer (C1 in Fig. 1) The most common reason for cases to fail this criterion is that the AOD never reaches background stratospheric AOD levels (near zero; 0.02-0.04 in the mid-visible), indicating measurements were not taken fully above the aerosol layer. Since the retrieval relies on the change in irradiance with altitude, incomplete profiles do not provide a sufficient change required to capture the aerosol signal.

The second requirement (C2 in Fig. 1) is to ensure that the true aerosol absorption be larger than the 3-D cloud effect known as horizontal flux divergence (see Fig 1 in C19). SSFR actually does not measure the absorption directly, but rather the decrease of the net flux F_λ^{net} from the top of the aerosol layer (TOL) to the bottom (BOL), or vertical flux divergence:

$$V_\lambda = \frac{(F_{\lambda,tol}^{net} - F_{\lambda,bol}^{net})}{F_{\lambda,tol}^\downarrow} = \frac{[(F_{\lambda,tol}^\downarrow - F_{\lambda,tol}^\uparrow) - (F_{\lambda,bol}^\downarrow - F_{\lambda,bol}^\uparrow)]}{F_{\lambda,tol}^\downarrow}, \quad (7)$$

which we normalized by the incident irradiance. V_λ is only the *vertical* part of the total flux divergence. The other part is the *horizontal* flux divergence, H_λ, which is not measured by SSFR. The true absorption, A_λ, is obtained from the *total* flux divergence:

$$A_\lambda = V_\lambda - H_\lambda. \tag{8}$$

If the condition $|H_\lambda| << |V_\lambda|$ (see section 3.1.2 in C19), then $A_\lambda \approx V_\lambda$, and the vertical flux divergence measured by SSFR can be used in lieu of the true absorption. The first step to check that this requirement is met is to calculate V_λ from the linear fit in equations (5) and (6):

$$V_\lambda = \frac{AOD_{532}^{max} * (b_\lambda^{\uparrow} - b_\lambda^{\downarrow})}{a_\lambda^{\downarrow}} \quad , \tag{9}$$

where $\mathrm{AOD}_{532}^{\mathrm{max}}$ is the AOD at the bottom of the spiral (just above the cloud), and a_λ, b_λ are the slope and intercept of the linear fit lines. The second step is to estimate H_λ. Neglecting its weak wavelength dependence (Song et al., 2016), we instead use H_∞, the value of H_λ at large wavelengths. As described in C19, H_∞ can be determined using measurements of AOD_λ and V_λ: the AOD decreases with increasing wavelength, and therefore the true aerosol absorption decreases as well; as AOD_λ reaches zero, so does A_λ. When this happens, any non-zero measured value of V_λ must originate from H_λ because $A_\lambda = 0 = V_\lambda + H_\lambda$. Since this occurs at long wavelengths, the vertical flux divergence $V_{\lambda \to \infty}$ yields H_∞. In practice, we obtain H_∞ from the intercept of the regression between AOD_λ and V_λ.

To determine the relative amount of absorption to horizontal flux divergence, C19 developed a unitless metric (i_λ) that determines whether the case is viable for an aerosol retrieval. i_λ is defined as:

$$i_\lambda = \frac{H_\infty}{V_\lambda - H_\infty}, \tag{10}$$

If $i_\lambda > 0.3$, then the condition $|H_\lambda| << |V_\lambda|$ is not met, and the case is not considered viable for a subsequent retrieval.

The final criteria (C3 in Fig 1.), the measured albedo at the cloud top (Bottom of Layer, BOL) and above the aerosol layer (Top of Layer, TOL) shown in 3b must be consistent in the limit of zero AOD. As the aerosol absorption decreases with increasing wavelength, the ratio between the measured albedo at the cloud top (BOL) and above the aerosol layer (TOL) must shift closer and closer to 1. Analogous to the determination of $H_\infty$and illustrated in Figure 2c, we determine AR_∞ as the intercept between the TOL and BOL albedo ratio and the AOD:

In the limit of: $\lambda \to \infty$:

$$lim_{AOD(\lambda)\to 0} \frac{albedo_{\lambda,TOL}}{albedo_{\lambda,BOL_\lambda}} \equiv AR_\infty. \quad (11)$$

AR_∞ is our final criterion, and any deviation larger than 0.1 from 1.0 (i.e., the intercept must fall between 0.9 and 1.1) indicates that other factors affect the data besides the aerosol absorption. For example, a changing cloud field could change the albedo between the beginning and end of the spiral, and the aerosol retrieval might wrongly attribute this change to aerosol absorption. To summarize, the criteria each case must pass are:

C1. There must be valid data from both SSFR and 4STAR throughout the entire aerosol profile. Cases cannot be used within the retrieval if there is a lack of data due to aircraft flight pattern, ALP malfunction, or AOD data flagged for bad quality.

C2. $|i_\lambda|$ must be below 0.3 to ensure that the aerosol absorption is large enough compared to the horizontal flux divergence so that an aerosol retrieval is possible.

C3. AR_∞ must fall between 0.9 and 1.1 to ensure that the spectral albedo is consistent both above and below the aerosol layer.

Both the filters and the criteria are designed to control for any rapidly changing, potentially inhomogeneous cloud field encountered during ORACLES. Table 1 presents the C2 and C3 criteria and retrieval status of SSA_λ and g_λ for spiral cases completed in 2016 and 2017 that passed C1. The criteria for which a case fails is indicated in red text. In 2016, five spiral profiles out of 18 met all criteria, while four out of 23 met the criteria in 2017. Table 2 provides the UTC, latitude, and longitude ranges for each successful spiral profile.

2.2.2 Retrieval Algorithm

If a spiral irradiance profile has passed every criteria metric, the aerosol property retrieval is run. The retrieval, described in detail in C19, is based on statistical probabilities between the calculated model irradiance profiles and the measured irradiance profiles. The retrieval process is similar to curve-fitting, where we vary the parameters in question (i.e. SSA and *g*) until the radiative transfer model (RTM) calculations best fit the measured data.

The SSA and *g* retrieval is performed with the publicly available 1-dimensional (1D) RTM DISORT 2.0 (Stamnes et al., 2000) with SBDART for atmospheric molecular absorption (Ricchiazzi et al., 1998) within the libRadtran library (Emde et al., 2016; libradtran.org). The RTM is run with 6 streams, assumes a Henyey Greenstein Phase function, and no delta-Eddington scaling is applied, all of which contribute to the inherent uncertainty within the RTM (Boucher et al., 1999). For each wavelength, we use the RTM to progress through pairs of SSA and *g* and calculate the upwelling, downwelling, and net irradiance profiles for each pair. For each {SSA, *g*} pair calculation, a probability is assigned to every SSFR data point in the profile according to the difference between the calculation and the measurement based on an assumed Gaussian distribution that represents the SSFR measurement uncertainty. The overall probability of a specific {SSA, *g*} pair given the SSFR irradiance measurements is the product of the individual probabilities for each data point; the {SSA, *g*} pair with the highest overall probability between all three profiles (upwelling, downwelling, net) is the retrieval result for that wavelength. The inclusion of the net profile is an expansion upon the method described in C19. The net irradiances provide a direct absorption constraint on the SSA retrieval, whereas the asymmetry parameter retrieval draws primarily upon the upwelling and downwelling fluxes.

In addition to the aerosol property pairs of {SSA, g}, the RTM ingests the spectral cloud top albedo from SSFR (set as the surface within the model at the measured altitude, around 2 km) and the aerosol extinction profile derived from the 4STAR AOD profile. The AOD profile has been conditioned such that the profile decreases monotonically to eliminate any unphysical extinction values (i.e., negative extinction). Any remaining AOD above the aerosol layer is allocated to a layer extending to an altitude of 15,000 m.

We modified the standard tropical atmosphere included in the libRadtran package (Andersen et al., 1986) to include the column water vapor measurements taken by the NASA P3 hygrometer from the level of the cloud top to the maximum altitude of the spiral; the values at altitudes that are not informed by aircraft measurements are set to the standard tropical atmosphere values. The full water vapor column was then scaled to the water vapor value retrieved with 4STAR. The column ozone amount in the standard tropical atmosphere is also scaled by the column ozone amount retrieved with 4STAR. As mentioned in section 2.2.1, the measured irradiances are corrected to the SZA at the midpoint of the spiral to account for the changing solar position during the spiral. For consistency, the SZA within the RTM is set to the same SZA of the spiral midpoint.

Table 2 lists, for each spiral case, the UTC, latitude, longitude albedo at 500 nm, mean SZA, AOD at 500 nm, column water vapor, and column ozone.

For 4 cases, the retrieval is possible only for SSA_λ and not for g_λ. This occurs when the irradiance profiles a) did not have enough data points and/or b) are subject to scene inhomogeneities despite the filters and criteria described in the previous section. The g retrieval is less sensitive than the SSA retrieval since the effect of g is smaller than that of SSA on the irradiance profile. For these specific cases, the retrieval is modified such that g is an input to the retrieval rather than a variable, and SSA is the only retrieved parameter. For each wavelength, the input of g is set to the mean value from the cases for which we had valid g retrievals. Table 1 lists which properties (SSA and g; SSA only) were retrieved for each case.

2.3 DARE

2.3.1 DARE Calculations

The retrieved pairs of SSA_λ and g_λ serve as the aerosol properties for the $DARE_\lambda$ calculations that the parameterizations are based upon. $DARE_\lambda$ can be calculated at any level. We focus on the TOL calculations since they will resemble those calculated at the tropopause which is used as a metric for the cooling/warming impact of aerosols (e.g. Forster et al., 2007.)

For each pair of retrieved SSA_λ and g_λ, we calculate instantaneous $DARE_\lambda$ for SZAs from 0° to 80° with a 10-degree resolution for a range of albedo and AOD values. Since the SSA_λ and g_λ retrievals are valid only for the shortwave wavelength range ($\lambda \leq 781$ nm), we extend to longer wavelengths (up to 2100 nm) as described in detail in Appendix A.

Finally, the albedo must be generalized to all SZAs for a range of albedo spectra to be used within the $DARE_\lambda$ calculations. Since we measure albedo only at a single SZA, we must use the RTM to determine the spectral shape and magnitude of the albedo at each SZA. We make this transition via a cloud retrieval; cloud properties of effective radius and cloud optical thickness (COT) are retrieved from the original cloud top albedo spectrum measured by SSFR at the bottom of the spiral. The effective radius is then held constant and the albedo spectra are calculated for a range of COTs at each SZA. Specific details of the albedo calculations can be found in Appendix A.

At each SZA, the RTM is run twice for each set of AOD values and cloud albedo spectra: with and without the aerosol layer included. The difference between the two runs is the $DARE_\lambda$. The calculations are completed for wavelengths between 350 and 2100 nm; the integration of the $DARE_\lambda$ spectrum provides broadband DARE. This is done for each pair of SSA_λ and g_λ.

2.3.2 Parameterizations

In the past, the Radiative Forcing Efficiency served the purpose of scaling measurements to larger regions and into climate models. However, the RFE excludes both the dependence of DARE on cloud albedo and the non-linearities of the DARE-AOD relationship. Our first goal was to develop a parameterization that builds upon the RFE concept and generalizes it to explicitly include the dependencies and non-linearities that the RFE excludes while maintaining simplicity. The parameterization (P_{DARE}) provides a broadband DARE estimate with minimal inputs in the form:

$$DARE = P(AOD_{550}, \alpha_{550}) = L(\alpha_{550}) * AOD_{550} + Q(\alpha_{550}) * AOD_{550}^2 \quad (12)$$

where L and Q are the parameterization coefficients and α_{550nm} and AOD_{550nm} are required inputs of 550 nm albedo and 550 nm AOD, respectively. P_{DARE} has the significant advantage that the complexities of transitioning from narrowband to broadband for many parameters are incorporated into the parameterization coefficients, allowing for use across regional spatial scales for biomass burning aerosol since minimal information is required as input. Of course, the parameterization is only applicable for the region where the measurements were taken. It also cannot be generalized to apply for a different aerosol type.

Our second goal was to increase the level of complexity of the P_{DARE} parameterization by including the additional constraint of the aerosol SSA. While P_{DARE} requires minimal input, the more advanced parameterization, PX_{DARE}, includes the 550 nm SSA as an additional parameter; this decreases the variability between cases. PX_{DARE} is in the form:

$$DARE = PX(AOD_{550}, \alpha_{550}, \Delta SSA_{550}) = P(AOD_{550}, \alpha_{550}) + \Delta(AOD_{550}, \alpha_{550}, \Delta SSA_{550}), \quad (13)$$

where the first term on the right-hand side is P_{DARE} (Equation 12) and the second term (delta term) represents the change in DARE due to varying SSA.

The coefficients of P_{DARE} and PX_{DARE} are determined based on the DARE calculations performed for each case with the associated pair of SSA_λ and g_λ, with the end result of two parameterizations that empirically represent the relationship between

DARE and its driving parameters while capturing the variability between individual cases. Further details of the P_{DARE} and PX_{DARE} development are best understood in conjunction with result figures and explained in further detail in Section 3.2.

3. From Aerosol Properties to DARE

3.1 Aerosol Properties

Figure 3a shows the retrieved asymmetry parameter values for each case with sufficient sensitivity. The red dashed line represents the average spectrum, where the error bars are calculated by propagating the uncertainty of each individual retrieval (shown in Appendix E). The average spectrum is used in the SSA retrievals for cases that did not have sufficient sensitivity to retrieve g.

The asymmetry parameter decreases with increasing wavelength more rapidly than found in AERONET retrievals from sites in the SE Atlantic (São Tomé, Ascension Island and Namibia; Appendix B, Fig B2). The AERONET retrieval algorithm is fundamentally different from the one used here. The AERONET operational inversion method assumes a size-independent complex refractive index (Dubovik and King, 2000), which can potentially lead to errors in the retrieved size distribution from which the optical properties are determined (Dubovik et al., 2002; Dubovik et al., 2006; Chowdhary et al., 2001). At 550 nm, the average g value is 0.52; by 660 nm, g has dropped to 0.43. Simple Mie calculations, shown in Appendix B, confirm that this spectral dependence is possible with a particular fine to coarse mode aerosol ratio. In addition, the AERONET sites are located at the perimeter of the ORACLES study region: At the very north (São Tomé), west (Ascension) and southeast (Namibia) ends of where the P3 flew. As such, the aerosol measured at the AERONET sites might actually differ from that measured during our retrievals.

Figure 3b shows the retrieved SSA spectra from each successful spiral case, and the mean retrieved SSA and g for each wavelength are presented in Table 3. Our retrievals of SSA range from 0.78 to 0.88 at 550 nm, with an average value of 0.83. The red spectrum shows the mean of all cases. The SSA retrieved through our new method is spectrally flatter than reported from the SAFARI 2000 campaign, which took place in the southeast region of the ORACLES measurement domain (Eck et al., 2003; Haywood et al., 2003; Russell et al., 2010). The SAFARI SSA values tend to be higher at the shorter wavelengths (i.e. < 550 nm), and they decrease more rapidly with increasing wavelength. The mean retrieved SSA values shown here are within the range of the 550 nm ORACLES 2016 SSA values from multiple instruments presented in Pistone et al. (2019), but are lower than most values from SAFARI 2000 (Haywood et al., 2003; Johnson et al., 2008; Russell et al., 2010). However, the mean SSA is close to the 0.85 value reported by Leahy et al. (2007). The lowest retrieved 550nm SSA value is only slightly lower than that reported by Johnson et al., 2008 for the Dust and Biomass-burning Experiment (DABEX): 0.78 compared to 0.81.

Figure 4 compares our retrieved values of SSA to the *in situ* column average for a) 450 nm b) 530 nm and c) 660 nm for all cases where such a comparison was possible. The *in situ* measurements are taken from a three-wavelength nephelometer (TSI 3563) and a three-wavelength particle soot absorption photometer (PSAP) (Radiance Research). The combination of scattering from the nephelometer and absorption from the PSAP provides SSA. SSA is calculated as the ratio of scattering from the nephelometer to the sum of scattering (again from the nephelometer) and absorption (from the PSAP). In order to best compare the retrieved values to the *in situ* values of SSA, the *in situ* measurements throughout the spiral profile are weighted by the weighting function, obtained by the transmittance, and then averaged to obtain a column value of SSA. Further details of the transmittance-weighted averaging can be found in Appendix C.

Although there are many factors that control aerosol SSA such as emission state, source location, distance from the source, and age (Haywood et al., 2003; Eck et al., 2013; Konovalov et al., 2017; Dobracki et al., 2020 in prep), the values we find here are well within the range of SSA values reported by other ORACLES instruments (Pistone et al., 2019). As seen in Figure 4, the mean SSFR/4STAR retrieved SSA value tends to be slightly lower than the in-situ mean (shown by the blue curve on x- and y- axis). However, there does not seem to be a distinct correlation or anti-correlation for these cases, especially considering the uncertainties. This is consistent with the results shown in Pistone et al. (2019), which also showed no distinct correlation between the SSA derived or measured by different instruments (top row in Figure 8).

It is important to note that the error bars shown in Figure 4 reflect different values between the instruments: the *in situ* error bars represent the standard deviation of the entire column, whereas the SSFR-retrieved error bars represent the error estimate of the retrieval. The *in situ* measurements provide a range of SSA, and the standard deviation illustrates the variability throughout the aerosol layer. Conversely, the SSFR/4STAR retrieval provides only one value of SSA with the associated retrieval uncertainty for the entire layer. We cannot, however, detect any altitude dependence of SSA that may be present, such as suggested by Wu et al. (2020) and Dobracki et al. (2020).

In addition, new, more accurate (compared to filter-based *in situ* measurements), cavity ring down and photo acoustic spectrometry instrumentation has recently been deployed to the SE Atlantic during the CLARIFY-2017 deployment. Davies *et al*. (2019) performed an analysis of the SSA of aerosol dominated by biomass burning aerosol using such instrumentation and found mean SSA values of 0.84, 0.83 and 0.81 at interpolated wavelengths of 467, 528, and 652 nm respectively. These values are included in Figure 4 (dashed cyan line) to highlight the agreement with the results of this work. Wu *et al*. (2020a) extended this analysis by examining the BBA in the free troposphere, finding a mean and variability in BBA SSA of 0.85 ± 0.02 and 0.82±0.04 at 405 and 658 nm with evidence that the BBA at higher altitudes in the free troposphere is less absorbing. These results appear entirely consistent with those derived here.

3.2 DARE Parameterizations

The first (basic) parameterization P_{DARE} uses only two input parameters: AOD_{550} (mid-visible optical thickness) and α_{550} (scene or cloud albedo below the aerosol layer). The L and Q coefficients from Eq 12 are derived from the nine individual cases (described in section 3.3.1) where the corresponding fit coefficients for each of the cases are averaged to create the P_{DARE} parameterization coefficients:

$L_0 = \frac{1}{9}\sum_{i=1}^{9} l_{0,i}$; $L_1 = \frac{1}{9}\sum_{i=1}^{9} l_{1,i}$; $L_2 = \frac{1}{9}\sum_{i=1}^{9} l_{2,i}$,

$Q_0 = \frac{1}{9}\sum_{i=1}^{9} q_{0,i}$; $Q_1 = \frac{1}{9}\sum_{i=1}^{9} q_{1,i}$; $Q_2 = \frac{1}{9}\sum_{i=1}^{9} q_{2,i}$.

The coefficients l_0, l_1, l_2, q_0, q_1, q_2 are the linear (*l*) and quadratic (*q*) coefficients of second-order polynomial fits to radiative transfer calculations for the DARE dependence on AOD_{550} of the *individual* cases as expressed in Eq 12 for the *average*, which simultaneously capture the dependence on α_{550} as follows:

$$l(\alpha_{550}) = l_0 + l_1 * \alpha_{550} + l_2 * \alpha_{550}^2, \quad (14)$$

$$q(\alpha_{550}) = q_0 + q_1 * \alpha_{550} + q_2 * \alpha_{550}^2, \quad (15)$$

The overall P_{DARE} coefficients are tabulated for each solar zenith angle *SZA*={0°, 5°, …, 80°} (see Table 4a).

Figure 5a shows the dependence of $DARE = P(AOD_{550}, \alpha_{550})$ on the two input parameters for one specific SZA. DARE is shown in percent of top-of-atmosphere irradiance[1], $S_0 * cos\ (SZA)$, where $S_0 = 1361$ W/m^2. It is clearly non-linear with respect to both input parameters, illustrating the need for a quadratic representation. However, the RFE from which P_{DARE} originates is still encapsulated in this parameterization as:

$$RFE = \frac{dP(AOD_{550}, \alpha_{550})}{dAOD_{550}}\Big|_{AOD_{550}=0} = L(\alpha_{550}), \quad (16)$$

which is the slope of the black line at the origin in Figure 5a. For an underlying albedo of 0, this reduces to $RFE = L_0$. In this sense, the full parameterization P_{DARE} generalizes RFE.

Whereas the black lines in Figure 5a and 5b show the average ORACLES parameterization (i.e. P_{DARE}) from Table 4a, the colored lines show the contributing 9 cases, sorted by 550 nm SSA. It is apparent that the SSA introduces considerable case-to-case variability, especially for large albedos (Fig. 6), both in terms of the critical albedo (Fig. 7) and in terms of the magnitude of the DARE.

Figure 6 shows the same as Figure 5b, but here as the difference between the DARE for individual cases and P_{DARE}, (which represents the case-average DARE) expressed as a percentage difference in incident TOA solar flux. The ±σ range of variability (essentially the root mean square (RMS) difference, shown as dashed black lines in Figure 7) is calculated from the standard deviation of this difference across all nine cases enumerated by *c*:

[1] Supplementary material includes all necessary coefficients for the parameterization as well as the code necessary to reconstruct them.

$$\sigma = \sqrt{\frac{1}{8}\sum_{c=1}^{9}(DARE_c - \overline{DARE})^2}. \quad (17)$$

This serves as a metric for the case-to-case variability, which increases with the scene albedo and AOD. For example, the possible range in DARE for a mid-visible albedo of 0.6 and an AOD of 0.75 (*SZA*=20°) would be about 10±2% (or 136±27 Wm^{-2}). This is *without* accounting for the uncertainty in the input parameters AOD and scene albedo, which have to be propagated through the parameterization via $dP/dAOD$ and $dP/d\alpha$. The uncertainty of 27 Wm^{-2} in brackets above can be interpreted as the uncertainty in DARE due to insufficient knowledge of SSA, which drives the case-to-case variability: in Figures 5 and 6, the highest (lowest) SSA values correspond to the lowest (highest) DARE.

The extended parameterization PX_{DARE} (equation 13) includes the SSA effect on DARE explicitly through an addition term not included in the P_{DARE} parameterization (equation 12): $\Delta(AOD_{550}, \alpha_{550}, \Delta SSA_{550})$.

In order to quantify the effect of SSA by this term, it is convenient to start with the dependence of the critical albedo on SSA (Figure 7). To first approximation, this dependence can be represented by a linear fit. The critical albedo also weakly depends on the AOD, and rather strongly on the SZA (not shown; for example, it can attain 0.6 at low Sun elevations) (Boucher et al., 1999). In contrast with the SSA, the asymmetry parameter does not drive the critical albedo in any discernible way, nor does it explain the deviation of the case-specific critical albedo from the fit line.

In analogy to the SSA dependence of the critical albedo, the case-specific deviations of DARE from the case-average DARE (Figure 6) can be represented as linear functions $\Delta(\alpha, SSA)$ (Figure 8a). Here, this is done by defining the DARE perturbation $\Delta(SSA)$ at two specific albedos: (1) at the case-average critical albedo (i.e. the albedo where DARE changes sign in Figure 7), and (2) an albedo of 1 (maximum albedo):

$$\Delta_{crit} = \Delta\left(AOD_{550}, \alpha_{550}^{crit}, \Delta SSA_{550}\right) = C(AOD_{550}) * \Delta SSA \quad (18)$$

$$\Delta_{max} = \Delta(AOD_{550}, \alpha_{550}^{max}, \Delta SSA_{550}) = D(AOD_{550}) * \Delta SSA \quad (19)$$

where C and D are the slopes of the fit lines of $\Delta(\alpha, SSA)$and ΔSSA is the difference between the case-specific SSA and the case-average SSA ($\overline{SSA}$, 0.83). The colored dots in Figure 8a show Δ_{crit} and Δ_{max}, while Figure 8b shows how the coefficients *C* and *D* depend on the AOD. This dependency can be represented as:

$$C(AOD) = C_1 * AOD + C_2 * AOD^2 \quad (20)$$

$$D(AOD) = D_1 * AOD + D_2 * AOD^2, \quad (21)$$

where C_1, C_2, D_1, and D_2 (and the relative uncertainties for the Δ_{crit} and Δ_{max} terms) are tabulated in Table 4b for all solar zenith angles. Inserting Eqs. 20 into 18 and 21 into 19, the perturbations Δ_{crit} and Δ_{max} become:

$$\Delta_{crit}(AOD_{550}, SSA_{550}) = (C_1 * AOD + C_2 * AOD^2) * (SSA - \overline{SSA}) \quad (22)$$

$$\Delta_{max}(AOD_{550}, SSA_{550}) = (D_1 * AOD + D_2 * AOD^2) * (SSA - \overline{SSA}) \quad (23)$$

The perturbation at *any* albedo between the critical albedo and 1 is simply calculated as:

$$\Delta(\alpha) = \frac{\alpha - \alpha_{crit}}{1 - \alpha_{crit}} * \Delta_{max} + \frac{1 - \alpha}{1 - \alpha_{crit}} * \Delta_{crit} \,, \quad (24)$$

while $\Delta(\alpha) = \Delta_{crit}$ for $\alpha < \alpha_{crit}$.

Equations 21, 22, 23, and 24 are used collectively to determine the additional term for the PX_{DARE} parameterization (Eq. 13). If SSA is known in addition to AOD and scene albedo, then PX_{DARE} captures DARE to greater fidelity than does P_{DARE}. This is shown by the case-to-case variability in Figure 9, expressed as the difference between the DARE for the individual cases $PX(AOD_{550}, \alpha_{550}, \Delta SSA_{550})$ in analogy to Figure 6. The $\pm\sigma$ range of variability in Figure 9 is much smaller than that in Figure 6, showing that the uncertainty in PX_{DARE} (±0.5% at an albedo of 0.3 of the incident irradiance at TOA) is significantly below the unresolved variability in P_{DARE} due to an unknown SSA (±1.2% at an albedo of 0.3, up to 2% at an SZA of 20°).

Beyond the case-to-case variability, Figure 10 confirms that including the SSA information in PX_{DARE} does in fact reproduce DARE well for each individual case, as illustrated by the agreement between the solid (PX_{DARE}) and the individual case RTM-calculated DARE. The residuals between the direct RTM DARE output and DARE estimated using P_{DARE} and PX_{DARE} (shown as contours in Figure 11a and Figure 11b) provide an estimate of the overall uncertainties inherent within the parameterizations.

As Figure 11a shows, the residuals of PX_{DARE} are significantly smaller than those of P_{DARE}. Both P_{DARE} and PX_{DARE} have small uncertainty contributions from a number of factors (e.g., measurement uncertainty of SSFR, RTM uncertainty, conversion and extrapolation from spectrally resolved retrievals to broadband values, the uncertainty of the quadratic fit leading to the *L* and *Q* coefficients, and the uncertainty in the fits leading to the *C* and *D* coefficients), but P_{DARE} also encompasses the variability due to SSA which leads to a much larger uncertainty in P_{DARE} than PX_{DARE}.

4. Summary and Interpretation

In this paper, we systematically linked aircraft observations of spectral fluxes to aerosol optical thickness and other parameters, using 9 cases from the 2016 and 2017 ORACLES campaigns. This observationally-driven link is expressed by two parameterizations of the shortwave broadband DARE, (1) in terms of the mid-visible AOD and scene albedo (P_{DARE}), and (2) in terms of the mid-visible AOD, scene albedo, and aerosol SSA (PX_{DARE}). These parameterizations can be used to translate from AOD and scene albedo (optionally also from SSA) to DARE directly, bypassing radiative transfer calculations that are usually required to arrive at DARE from observations. This is advantageous when satellite retrievals provide only limited information such as AOD and scene albedo (by way of cloud fraction and optical thickness), but not aerosol microphysics, hygroscopic growth, or optical properties. However, this parameterization only captures the natural variability of the study region as sampled. It therefore does not necessarily represent the entire southeast Atlantic, let alone during times beyond the ORACLES campaigns. Despite this caveat, one could interpret the parameterization as the start of a DARE climatology built on two (or three) driver variables. Additional observations extending the statistics to other regions and time periods could easily be added to this framework. For example, the 2018 ORACLES data will be incorporated in a separate paper.

We find that the two parameterizations reproduce the case-specific DARE to different degrees. The majority of the case-to-case variability within the ORACLES DARE dataset is attributable to the dependence on AOD and scene albedo. Using just these two variables to span the first parameterization, P_{DARE}, the RMS bias of the case-specific DARE with respect to the parameterized baseline is 1-2% of the incident radiation for an SZA of 20° and an AOD of 0.75 (Figure 6), with a DARE value of 10% of the incident radiation for a scene albedo of 0.6 (Figure 5b). Translated into flux units, the DARE for this constellation of scene parameters is 136±27 W m^{-2}, where the range of uncertainty stems from the unexplained case-to-case variability as obtained from the RMS bias. In other words, this parameterization leads to 20% DARE uncertainty due to the variability of the system caused by factors *other* than AOD and scene albedo. If satellites only provided AOD and scene albedo, this would be the uncertainty of the derived DARE (leaving the retrieval uncertainties of AOD and albedo aside for the moment). In reality, the variability is likely even larger than captured with our limited samples, so this estimate is a lower bound on the DARE variability.

Fortunately, our research showed that we can actually explain more of the case-to-case variability by introducing the mid-visible SSA as third parameter in an extended parameterization PX_{DARE}. This reduces the variability by a factor of 4 by explicitly resolving the case-to-case variability via SSA: a DARE value of 136±6.8 Wm^{-2} corresponds to an SSA of 0.83 (campaign average at 550 nm), whereas 0.81 (typical low SSA value encountered during ORACLES) yields DARE of 177±10.6 Wm^{-2}. The remaining uncertainty (about 5%) is due to variability drivers beyond AOD, scene albedo and SSA, such as variable aerosol microphysics or hygroscopicity. It also encompasses the measurement uncertainty of SSFR and 4STAR.

Interestingly, the mid-visible asymmetry parameter (also retrieved for most cases) is not a significant driver of the case-to-case variability. However, the retrieved spectra of SSA and asymmetry parameter can be useful for future satellite retrievals of cloud and aerosol optical thickness in the study region. Since these retrievals are directly tied to the radiative fluxes, they work without assumptions about the scattering phase function, size distribution, or aerosol type, nor do they require smoothness constraints. However, an optical closure study that involves in-situ measurements of aerosol microphysics and optical properties in conjunction with Mie calculations is required before our results can be of practical use, especially at wavelengths beyond the visible range where our retrieval uncertainties grow large. Our asymmetry parameter spectra fall off faster with wavelength than usually assumed based on land-based observations, which may be an indication that there is less coarse mode in the ORACLES measurements, which are almost exclusively over ocean.

We cannot judge whether our approach will be useful for predictive models, which usually follow the "bottom-up" paradigm, i.e., they arrive at DARE starting from detailed aerosol and cloud properties via radiative transfer calculations. At the very least, the agreement between the absolute values and spectral dependence of the SSA and asymmetry parameter retrievals coming out of our and other ORACLES/LASIC/CLARIFY-2017/AEROCLO-Sa studies (Zuidema et al., 2016) such as Davies et al. (2019) and Wu et al. (2020) will provide robust constraints of the aerosol optical properties in a range of models. However, we also anticipate that our parameterized, observationally-based DARE could serve as a simple, built-in closure for the calculated DARE, adding a "top-down" model constraint, or even prove useful for model tuning.

Our paper is focused on instantaneous DARE and stops short of providing an "all-ORACLES" (diurnally-integrated) DARE estimate. A promising approach in this regard is to use geostationary satellite retrievals of cloud and aerosol properties (Peers et al., 2020) in conjunction with in-situ aircraft data and radiative transfer calculations. Alternatively, one can use the satellite radiances to extrapolate from the spatially and temporally limited aircraft observations to obtain regional estimates of the diurnally-integrated DARE, circumventing the satellite retrievals. This approach, already underway within our group, builds on the *P* or PX parameterization, specifically by using albedo data from the geostationary Spinning Enhanced Visible and Infrared Imager (SEVIRI) in combination with ORACLES AOD data from HSRL-2 and 4STAR (Chen et al., 2020 in preparation). A grid-box specific model-to-observation inter-comparison is also underway in the wider ORACLES team. ~~, and we expect that it will entail detailed radiative and optical closure efforts.~~ While we limited this paper to the above-layer (TOA) DARE, the radiative effect of aerosols on the layer itself (i.e., the heating rate) is also an important deliverable from ORACLES, which will be presented in a separate follow-up paper.

References

Anderson, Gail P., Shepard Anthony Clough, F. X. Kneizys, James H. Chetwynd, and Eric P. Shettle. AFGL atmospheric constituent profiles (0.120 km). No. AFGL-TR-86-0110. AIR FORCE GEOPHYSICS LAB HANSCOM AFB MA, 1986.

Boucher, O., Schwartz, S. E., Ackerman, T. P., Anderson, T. L., Bergstrom, B., Bonnel, B., Chylek, P., Dahlback, A., Fouquart, Y., Fu, Q., Halthore, R. N., Haywood, J. M., Iversen, T., Kato, S., Kinne, S., Kirkevag, A., Knapp, K. R., Lacis, A., Laszlo, I., Mishchenko, M. I., Nemesure, S., Ramaswamy, V., Roberts, D. L., Russell, P., Schlesinger, M. E., Stephens, G. L., Wagener, R., Wang, M., Wong, J., and Yang, F.: Intercomparison of models representing direct shortwave radiative forcing by sulfate aerosols, J. Geophys. Res.-Atmos., 103, 16979–16998, 1998

Chand, D., Wood, R., Anderson, T. L., Satheesh, S. K., and Charlson, R. J.: Satellite-derived direct radiative effect of aerosols dependent on cloud cover, Nat. Geosci., 2, 181–184, 2009.

Chowdhary, J., Cairns, B., Mishchenko, M., and Travis, L.: Retrieval of aerosol properties over the ocean using multispectral and multiangle photopolarimetric measurements from the Research Scanning Polarimeter, Geophys. Res. Lett., 28, 243–246, doi:10.1029/2000GL01178, 2001.

Cochrane, S. P., Schmidt, K. S., Chen, H., Pilewskie, P., Kittelman, S., Redemann, J., LeBlanc, S., Pistone, K., Kacenelenbogen, M., Segal Rozenhaimer, M., Shinozuka, Y., Flynn, C., Platnick, S., Meyer, K., Ferrare, R., Burton, S., Hostetler, C., Howell, S., Freitag, S., Dobracki, A., and Doherty, S.: Above-cloud aerosol radiative effects based on ORACLES 2016 and ORACLES 2017 aircraft experiments, Atmos. Meas. Tech., 12, 6505–6528, https://doi.org/10.5194/amt-12-6505-2019, 2019.

Coddington, O. M., Pilewskie, P., Redemann, J., Platnick, S., Russell, P. B., Schmidt, K. S.,and Vukicevic, T.: Examining the impact of overlying aerosols on the retrieval of cloud optical properties from passive remote sensing, J. Geophys. Res.-Atmos., 115, D10211, doi:10.1029/2009JD012829, 2010.

Davies, N. W., Fox, C., Szpek, K., Cotterell, M. I., Taylor, J. W., Allan, J. D., Williams, P. I., Trembath, J., Haywood, J. M., and Langridge, J. M.: Evaluating biases in filter-based aerosol absorption measurements using photoacoustic spectroscopy, Atmos. Meas. Tech., 12, 3417–3434, https://doi.org/10.5194/amt-12-3417-2019, 2019.

Deaconu, L. T., Waquet, F., Josset, D., Ferlay, N., Peers, F., Thieuleux, F., Ducos, F., Pascal, N., Tanré, D., Pelon, J., and Goloub, P.: Consistency of aerosols above clouds characterization from A-Train active and passive measurements, Atmos. Meas. Tech., 10, 3499–3523, https://doi.org/10.5194/amt-10-3499-2017, 2017.

de Graaf, M., Tilstra, L. G., Wang, P., and Stammes, P.: Retrieval of the aerosol direct radiative effect over clouds from spaceborne spectrometry, J. Geophys. Res.-Atmos., 117, D07207, doi:10.1029/2011JD017160, 2012.

Doherty, S. J., Saide, P., Zuidema, P., Shinozuka, Y., Ferrada, G., Mallet, M., Meyer, K., Painemal, D., Howell, S. G., Freitag, S., Smirnow, N., Dobracki, A., Podolske, J., Pfister, L., Ueyama, R., Nabat, P., Wood, R. and Redemann, J.: A summary and model-observation comparison of vertically-resolved aerosol and cloud properties over the Southeast Atlantic, in preparation.

Dobracki et al.: Understanding the Lifetime of Observed Biomass Burning Aerosol in the Free Troposphere, 2020 in preparation.

Dubovik, O., and King, M. D.: A flexible inversion algorithm for retrieval of aerosol optical properties from Sun and sky radiance measurements, J. Geophys. Res., 105, 20673–20696, 2000.

Dubovik, O., B. N. Holben,T. F. Eck, A. Smirnov, Y. J. Kaufman, M. D. King, D. Tanré, and I. Slutsker(2002), Variability of absorption and optical properties of key aerosol types observed in worldwide locations, *J. Atmos. Sci.*, **59**, 590–608, doi:10.1175/15200469, 2002.

Dubovik, O., et al. (2006), Application of spheroid models to account for aerosol particle nonsphericity in remote sensing of desert dust, J. Geophys. Res., 111, D11208, doi:10.1029/2005JD006619.

Dunagan, S., Johnson, R., Zavaleta, J., Russell, P., Schmid, B., Flynn, C., Redemann, J., Shinozuka, Y., Livingston, J., Segal Rozenhaimer, M.: Spectrometer for Sky-Scanning Sun-Tracking Atmospheric Research (4STAR): Instrument Technology. Remote Sensing. 5. 3872-3895. 10.3390/rs5083872, 2013.

Eck, T. F., Holben, B. N., Ward, D. E., Mukelabai, M. M., Dubovik, O., Smirnov, A., Schafer, J. S., Hsu, N. C., Piketh, S. J., Queface, A., Le Roux, J., and Slutsker, I.: Variability of biomass burning aerosol optical characteristics in southern

Africa during the SAFARI 2000 dry season campaign and a comparison of single scattering albedo estimates from radiometric measurements, J. Geophys. Res., 108(D13), 8477, doi:10.1029/2002JD002321, 2003.

Eck, T. F., Holben, B. N., Reid, J. S., Mukelabai, M. M., Piketh, S. J., Torres, O., Jethva, H. T., Hyer, E. J., Ward, D. E., Dubovik, O., Sinyuk, A., Schafer, J. S., Giles, D. M., Sorokin, M., Smirnov, A., and Slutsker, I.: A seasonal trend of single scattering albedo in southern African biomass-burning particles: Implications for satellite products and estimates of emissions for the world's largest biomass-burning source, J. Geophys. Res., 118, doi:10.1002/jgrd.50500, 2013.

Emde, C., Buras-schnell, R., Kylling, A., Mayer, B., Gasteiger, J., Hamann, U., Kylling, J., Richter, B., Pause, C., Dowling, T. and Bugliaro, L., The libRadtran software package for radiative transfer calculations (version 2.0.1), Geosci. Model Dev., 9, 1647–1672, doi:10.5194/gmd-9-1647-2016, 2016.

Ferrare, R. A., Burton, S. P.,Cook, A. L., Harper, D. B., Hostetler, C. A., Hair, J. W., Josset, D. B., Clayton, M., Fenn, M. A., Vaughan, M., and Hu, Y.: "Biomass Burning Aerosol Distributions over the Southeastern Atlantic Ocean measured by CALIOP and the NASA LaRC airborne High Spectral Resolution Lidar-2", American Geophysical Union, Fall Meeting 2018, abstract #A12C-06, https://ui.adsabs.harvard.edu/abs/2018AGUFM.A12C..06F/abstract. 2018.

Forster, P., V. Ramaswamy, P. Artaxo, T. Berntsen, R. Betts, D.W. Fahey, J. Haywood, J. Lean, D.C. Lowe, G. Myhre, J. Nganga, R. Prinn, G. Raga, M. Schulz and R. Van Dorland, 2007: Changes in Atmospheric Constituents and in Radiative Forcing. In: Climate Change 2007: The Physical Science Basis. Contribution of Working Group I to the Fourth Assessment Report of the Intergovernmental Panel on Climate Change [Solomon, S., D. Qin, M. Manning, Z. Chen, M. Marquis, K.B. Averyt, M.Tignor and H.L. Miller (eds.)]. Cambridge University Press, Cambridge, United Kingdom and New York, NY, USA.

Haywood, J.M., and Shine, K.P.: The effect of anthropogenic sulfate and soot aerosol on the clear sky planetary radiation budget. Geophys. Res. Letts., 22, 5, 603- 606, 1995.

Hansen, J., Sato, M., and Ruedy, R.: Radiative forcing and climate response. J. Geophys. Res., 102, 6831-6864, doi:10.1029/96JD03436, 1997.

Haywood, J., S. R. Osborne, P. N. Francis, A. Keil, P. Formenti, M. O. Andreae, and P. H. Kaye, The mean physical and optical properties of regional haze dominated by biomass burning aerosol measured from the C-130 aircraft during SAFARI 2000, *J. Geophys. Res.*, 108(D13), 8473, doi:10.1029/2002JD002226, 2003.

Haywood, J. M., Osborne, S. R., and Abel, S. J.: The effect of overlying absorbing aerosol layers on remote sensing retrievals of cloud effective radius and cloud optical depth, Q. J. Roy. Meteorol. Soc., 130, 779–800, 2004.

Hu, Y., Vaughan, M., Liu, Z., Powell, K., and Rodier, S.: "Retrieving Optical Depths and Lidar Ratios for Transparent Layers Above Opaque Water Clouds From CALIPSO Lidar Measurements," in *IEEE Geoscience and Remote Sensing Letters*, vol. 4, no. 4, pp. 523-526, Oct. 2007.doi: 10.1109/LGRS.2007.901085, 2007.

Johnson, B. T., Osborne, S. R., Haywood, J. M., and Harrison, M. A. J.: Aircraft measurements of biomass burning aerosol over West Africa during DABEX,J. Geophys. Res.,113, D00C06, doi:10.1029/2007JD009451, 2008.

Keil, A., and Haywood, J. M.: Solar radiative forcing by biomass burning aerosol particles during SAFARI 2000: A case study based on measured aerosol and cloud properties, J. Geophys. Res., 108(D13), 8467, doi:10.1029/2002JD002315, 2003.

Konovalov, I. B., Beekmann, M., Berezin, E. V., Formenti, P., and Andreae, M. O.: Probing into the aging dynamics of biomass burning aerosol by using satellite measurements of aerosol optical depth and carbon monoxide, Atmos. Chem. Phys., 17, 4513–4537, https://doi.org/10.5194/acp-17-4513-2017, 2017.

LeBlanc, S. E., Redemann, J., Flynn, C., Pistone, K., Kacenelenbogen, M., Segal-Rosenheimer, M., Shinozuka, Y., Dunagan, S., Dahlgren, R. P., Meyer, K., Podolske, J., Howell, S. G., Freitag, S., Small-Griswold, J., Holben, B., Diamond, M., Wood, R., Formenti, P., Piketh, S., Maggs-Kölling, G., Gerber, M., and Namwoonde, A.: Above-cloud aerosol optical depth from airborne observations in the southeast Atlantic, Atmos. Chem. Phys., 20, 1565–1590, https://doi.org/10.5194/acp-20-1565-2020, 2020.

Leahy, L. V., Anderson, T. L., Eck, T. F., and Bergstrom, R. W.: A synthesis of single scattering albedo of biomass burning aerosol over southern Africa during SAFARI 2000, *Geophys. Res. Lett.*, 34, L12814, doi:10.1029/2007GL029697, 2007.

Liu, Z., Winker, D., Omar, A., Vaughan, M., Kar, J., Trepte, C., Hu, Y., and Schuster, G.: Evaluation of CALIOP 532 nm aerosol optical depth over opaque water clouds, Atmos. Chem. Phys., 15, 1265–1288, https://doi.org/10.5194/acp-15-1265-2015, 2015.

Meyer, K., S. Platnick, L. Oreopoulos, and D. Lee.: Estimating the direct radiative effect of absorbing aerosols overlying marine boundary layer clouds in the southeast Atlantic using MODIS and CALIOP, J. Geophys. Res. Atmos., 118, 4801–4815, doi:10.1002/jgrd.50449. 2013.

Meyer, K., Platnick, S., and Zhang, Z.: Simultaneously inferring above-cloud absorbing aerosol optical thickness and underlying liquid phase cloud optical and microphysical properties using MODIS, J. Geophys. Res. Atmos., 120, 5524–5547, doi:10.1002/2015JD023128, 2015.

Meywerk, J., and V. Ramanathan, Observations of the spectral clear-sky aerosol forcing over the tropical Indian Ocean, J. Geophys. Res., 104,24359–24370, 1999.

Myhre, G., Samset, B. H., Schulz, M., Balkanski, Y., Bauer, S., Berntsen, T. K., Bian, H., Bellouin, N., Chin, M., Diehl, T., Easter, R. C., Feichter, J., Ghan, S. J., Hauglustaine, D., Iversen, T., Kinne, S., Kirkevåg, A., Lamarque, J.-F., Lin, G., Liu, X., Lund, M. T., Luo, G., Ma, X., van Noije, T., Penner, J. E., Rasch, P. J., Ruiz, A., Seland, Ø., Skeie, R. B., Stier, P., Takemura, T., Tsigaridis, K., Wang, P., Wang, Z., Xu, L., Yu, H., Yu, F., Yoon, J.-H., Zhang, K., Zhang, H., and Zhou, C.: Radiative forcing of the direct aerosol effect from AeroCom Phase II simulations, Atmos. Chem. Phys., 13, 1853–1877, https://doi.org/10.5194/acp-13-1853-2013, 2013.

ORACLES Science Team: Suite of Aerosol, Cloud, and Related Data Acquired Aboard P3 During ORACLES 2016, Version 1, NASA Ames Earth Science Project Office, Accessed at doi:10.5067/Suborbital/ORACLES/P3/2016_V1, 2017.

ORACLES Science Team: Suite of Aerosol, Cloud, and Related Data Acquired Aboard P3 During ORACLES 2017, Version 1, NASA Ames Earth Science Project Office, Accessed at doi: 10.5067/Suborbital/ORACLES/P3/2017_V1, 2019.

Peers, F., Francis, P., Abel, S. J., Barrett, P. A., Bower, K. N., Cotterell, M. I., Crawford, I., Davies, N. W., Fox, C., Fox, S., Langridge, J. M., Meyer, K. G., Platnick, S. E., Szpek, K., and Haywood, J. M.: Observation of absorbing aerosols above clouds over the South-East Atlantic Ocean from the geostationary satellite SEVIRI – Part 2: Comparison with MODIS and aircraft measurements from the CLARIFY-2017 field campaign, Atmos. Chem. Phys. Discuss., https://doi.org/10.5194/acp-2019-1176, in review, 2020.

Pistone, K., Redemann, J., Doherty, S., Zuidema, P., Burton, S., Cairns, B., Cochrane, S., Ferrare, R., Flynn, C., Freitag, S., Howell, S. G., Kacenelenbogen, M., LeBlanc, S., Liu, X., Schmidt, K. S., Sedlacek III, A. J., Segal-Rozenhaimer, M., Shinozuka, Y., Stamnes, S., van Diedenhoven, B., Van Harten, G., and Xu, F.: Intercomparison of biomass burning aerosol optical properties from in situ and remote-sensing instruments in ORACLES-2016, Atmos. Chem. Phys., 19, 9181 9208, https://doi.org/10.5194/acp-19-9181-2019, 2019.

Redemann, J., Pilewskie, P., Russell, P. B., Livingston, J. M., Howard, S., Schmid, B., Pommier, J., Gore, W., Eilers, J., and Wendisch, M.: Airborne measurements of spectral direct aerosol radiative forcing in the Intercontinental chemical Transport Experiment/Intercontinental Transport and Chemical Transformation of anthropogenic pollution, 2004, J. Geophys. Res., 111, D14210, doi:10.1029/2005JD006812, 2006.

Redemann, J., Wood, R., Zuidema, P., Doherty, S. J., Luna, B., LeBlanc, S. E., Diamond, M. S., Shinozuka, Y., Chang, I. Y., Ueyama, R., Pfister, L., Ryoo, J., Dobracki, A. N., da Silva, A. M., Longo, K. M., Kacenelenbogen, M. S., Flynn, C. J., Pistone, K., Knox, N. M., Piketh, S. J., Haywood, J. M., Formenti, P., Mallet, M., Stier, P., Ackerman, A. S., Bauer, S. E., Fridlind, A. M., Carmichael, G. R., Saide, P. E., Ferrada, G. A., Howell, S. G., Freitag, S., Cairns, B., Holben, B. N., Knobelspiesse, K. D., Tanelli, S., L'Ecuyer, T. S., Dzambo, A. M., Sy, O. O., McFarquhar, G. M., Poellot, M. R., Gupta, S., O'Brien, J. R., Nenes, A., Kacarab, M. E., Wong, J. P. S., Small-Griswold, J. D., Thornhill, K. L., Noone, D., Podolske, J. R., Schmidt, K. S., Pilewskie, P., Chen, H., Cochrane, S. P., Sedlacek, A. J., Lang, T. J., Stith, E., Segal-Rozenhaimer, M., Ferrare, R. A., Burton, S. P., Hostetler, C. A., Diner, D. J., Platnick, S. E., Myers, J. S., Meyer, K. G., Spangenberg, D. A., Maring, H., and Gao, L.: An overview of the ORACLES (ObseRvations of Aerosols above CLouds and their intEractionS) project: aerosol-cloud-radiation interactions in the Southeast Atlantic basin, Atmos. Chem. Phys. Discuss., https://doi.org/10.5194/acp-2020-449, in review, 2020.

Russell, P. B., Kinne, S. A., and Bergstrom, R. W.: Aerosol climate effects: Local radiative forcing and column closure experiments, *J. Geophys. Res.*, 102(D8), 9397– 9407, doi:10.1029/97JD00112, 1997.

Russell, P. B., Livingston, J. M., Hignett, P., Kinne, S., Wong, J., Chien, A., Bergstrom, R., Durkee, P. and Hobbs, P. V.: Aerosol-induced radiative flux changes off the United States mid-Atlantic coast: Comparison of values calculated from sunphotometer and in situ data with those measured by airborne pyranometer, J. Geophys. Res., 104(D2), 2289–2307, 1999.

Russell, P. B., Redemann, J., Schmid, B., Bergstrom, R. W., Livingston, J. M., Mcintosh, D. M., Ramirez, S. A., Hartley, S., Hobbs, P. V., Quinn, P. K., Carrico, C. M., Rood, M. J., Ostrom, E., Noone, K. J., Von Hoyningen-Huene, W., and Remer, L.: Comparison of Aerosol Single Scattering Albedos Derived by Diverse Techniques in Two North Atlantic Experiments., Journal of the Atmospheric Sciences 59.3, 609-19, 2002.

Russell, P. B., Bergstrom, R. W., Shinozuka, Y., Clarke, A. D., Decarlo, P. F., Jimenez, J. L., Livingston, J. M., Redemann, J., Dubovik, O., and Strawa, A.: Absorption Angstrom Exponent in AERONET and Related Data as an Indicator of Aerosol Composition., Atmospheric Chemistry and Physics 10.3: 1155-169, 2010.

Ricchiazzi, P., Yang, S., Gautier, C., and Sowle, D.: SBDART: A Research and Teaching Software Tool for Plane-Parallel Radiative Transfer in the Earth's Atmosphere, B. Am. Meteor.ol Soc., 79, 2101–2114, https://doi.org/10.1175/1520-0477(1998)079<2101:SARATS>2.0.CO;2, 1998.

Russell, P. B., J. Redemann, B. Schmid, R. W. Bergstrom, J. M. Livingston, D. M. Mcintosh, S. A. Ramirez, S. Hartley, P. V. Hobbs, P. K. Quinn, C. M. Carrico, M. J. Rood, E. Ostrom,K. J. Noone, W. Von Hoyningen-Huene, and L. Remer.: Comparison of Aerosol Single Scattering Albedos Derived by Diverse Techniques in Two North Atlantic Experiments., Journal of the Atmospheric Sciences 59.3, 609-19. 2002.

Russell, P. B., R. W. Bergstrom, Y. Shinozuka, A. D. Clarke, P. F. Decarlo, J. L. Jimenez, J. M. Livingston, J. Redemann, O. Dubovik, and A. Strawa.:Absorption Angstrom Exponent in AERONET and Related Data as an Indicator of Aerosol Composition., Atmospheric Chemistry and Physics 10.3: 1155-169. 2010.

Segal-Rosenheimer, M., Russell, P. B., Schmid, B., Redemann, J., Livingston, J. M., Flynn, C. J., Johnson, R. R., Dunagan, S. E., Shinozuka, Y., Herman, J., Cede, A., Abuhassan, N., Comstock, J. M., Hubbe, J. M., Zelenyuk, A., and Wilson, J.: Tracking elevated pollution layers with a newly developed hyperspectral Sun/Sky spectrometer(4STAR): Results from the TCAP 2012 and 2013 campaigns, J. Geophys. Res.-Atmos., 119, 2611–2628, https://doi.org/10.1002/2013JD020884, 2014.

Shinozuka, Y., Johnson, R. R., Flynn, C. J., Russell, P. B., Schmid, B., Redemann, J., Dunagan, S. E., Kluzek, C. D., Hubbe, J. M., Segal-Rosenheimer, M., Livingston, J. M., Eck, T. F., Wagener, R., Gregory, L., Chand, D., Berg, L. K., Rogers, R. R., Ferrare, R. A., Hair, J. W., Hostetler, C. A., and Burton, S. P.: Hyperspectral aerosol optical depths from TCAP flights, J. Geophys. Res.-Atmos., 118, 12180–12194, https://doi.org/10.1002/2013JD020596, 2013.

Shinozuka, Y., Saide, P. E., Ferrada, G. A., Burton, S. P., Ferrare, R., Doherty, S. J., Gordon, H., Longo, K., Mallet, M., Feng, Y., Wang, Q., Cheng, Y., Dobracki, A., Freitag, S., Howell, S. G., LeBlanc, S., Flynn, C., Segal-Rosenhaimer, M., Pistone, K., Podolske, J. R., Stith, E. J., Bennett, J. R., Carmichael, G. R., da Silva, A., Govindaraju, R., Leung, R., Zhang, Y., Pfister, L., Ryoo, J.-M., Redemann, J., Wood, R., and Zuidema, P.: Modeling the smoky troposphere of the southeast Atlantic: a comparison to ORACLES airborne observations from September of 2016, Atmos. Chem. Phys. Discuss., https://doi.org/10.5194/acp-2019-678, in review, 2019.

Song, S., Schmidt, K. S., Pilewskie, P., King, M. D., Heidinger, A. K., Walther, A., Iwabuchi, H., Wind, G., and Coddington, O. M.: The spectral signature of cloud spatial structure in shortwave irradiance, Atmos. Chem. Phys., 16, 13791–13806, https://doi.org/10.5194/acp-16-13791-2016, 2016.

Stamnes, K., Tsay, S.-C., Wiscombe, W., and Laszlo, I.: DISORT, a General-Purpose Fortran Program for Discrete-Ordinate-Method Radiative Transfer in Scattering and Emitting Layered Media: Documentation of Methodology, Tech. rep., Dept. of Physics and Engineering Physics, Stevens Institute of Technology, Hoboken, NJ 07030, 2000.

Twomey, S. (1977), Atmospheric Aerosols, Section 12.3, pp. 278-290, Elsevier Scientific Publishing Co., United Kingdom.

van der Werf, G. R., Randerson, J. T., Giglio, L., Collatz, G. J., Mu, M., Kasibhatla, P. S., Morton, D. C., DeFries, R. S., Jin, Y., and van Leeuwen, T. T.: Global fire emissions and the contribution of deforestation, savanna, forest, agricultural, and peat fires (1997– 2009), Atmos. Chem. Phys., 10, 11707–11735, doi:10.5194/acp10-11707-2010, 2010.

Wu, H., Taylor, J. W., Szpek, K., Langridge, J., Williams, P. I., Flynn, M., Allan, J. D., Abel, S. J., Pitt, J., Cotterell, M. I., Fox, C., Davies, N. W., Haywood, J., and Coe, H.: Vertical variability of the properties of highly aged biomass burning aerosol transported over the southeast Atlantic during CLARIFY-2017, Atmos. Chem. Phys. Discuss., https://doi.org/10.5194/acp-2020-197, in review, 2020.

Yu, H., Kaufman, Y. J., Chin, M., Feingold, G., Remer, L. A., Anderson, T. L., Balkanski, Y., Bellouin, N., Boucher, O., Christopher, S., DeCola, P., Kahn, R., Koch, D., Loeb, N., Reddy, M. S., Schulz, M., Takemura, T., and Zhou, M.: A review of measurement-based assessments of the aerosol direct radiative effect and forcing, Atmos. Chem. Phys., 6, 613–666, https://doi.org/10.5194/acp-6-613-2006, 2006.

Zhang, Z., Meyer, K., Yu, H., Platnick, S., Colarco, P., Liu, Z., and Oreopoulos, L.: Shortwave direct radiative effects of above-cloud aerosols over global oceans derived from 8 years of CALIOP and MODIS observations, Atmos. Chem. Phys., 16,2877-2900,doi:10.5194/acp-16-2877-2016,2016.

Zuidema, P., Redemann, J., Haywood, J., Wood, R., Piketh, S., Hipondoka, M., and Formenti, P.: Smoke and Clouds above the Southeast Atlantic Upcoming Field Campaigns Probe Absorbing Aerosol's Impact on Climate, B. Am. Meteorol. Soc., 97, 1131–1135, https://doi.org/10.1175/BAMS-D-15-00082.1, 2016.

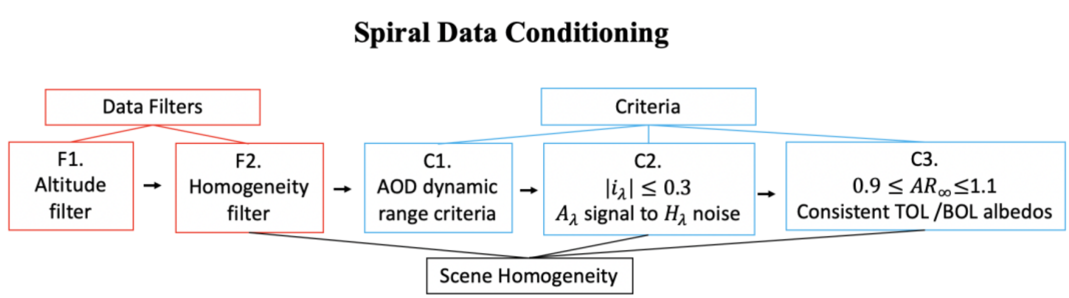

Figure 1: Data conditioning flow chart. First, the data is filtered vertically (i.e. data is removed) to F1) isolate the aerosol layer only and F2) isolate either cloudy or clear sky data such that the profile represents a homogeneous sky type. Once filtered, the data must pass 3 distinct criteria to ensure that C1) the full aerosol layer is captured C2) the effect of aerosol absorption on radiative fluxes is

much greater than that due to horizontal variability present and C3) the top-of-layer (TOL) and bottom of layer (BOL) albedos are mutually consistent.

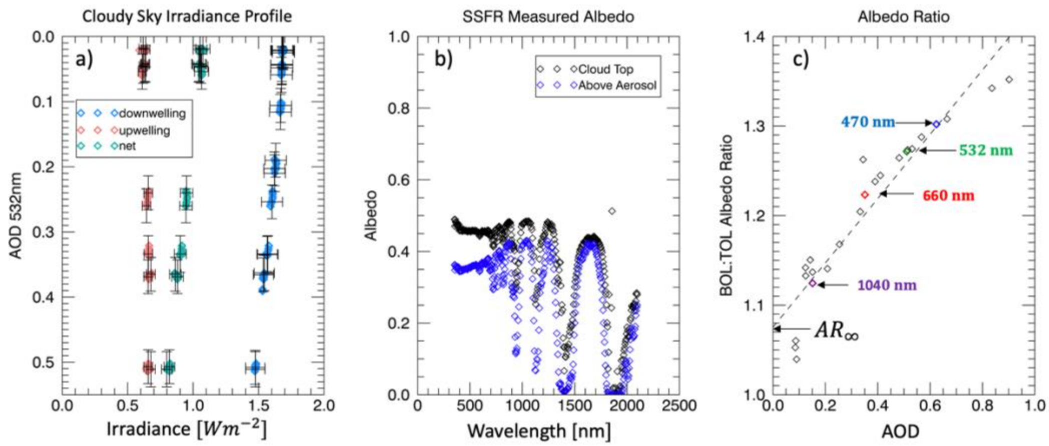

Figure 2: a) Above cloudy sky upwelling, downwelling, and net irradiance profiles shown versus the measured 532 nm AOD by 4STAR with associated measurement error bars for one example case. The AOD refers to the air above the aircraft and generally decreases with increasing aircraft altitude, hence the inverted y-axis. b) SSFR measured albedo spectrum at the bottom of the spiral (cloud top) and at the top of the spiral (above the aerosol layer. c) The ratio between the BOL and TOL albedo spectra (taken from Fig 2b) shown against the BOL AOD spectrum at the 4STAR wavelengths. The intercept of the fit line is criteria 3 (AR_∞); if the intercept deviates largely from 1.0, the case cannot be used for an aerosol retrieval. Select wavelengths are labelled to highlight the spectral importance of this method.

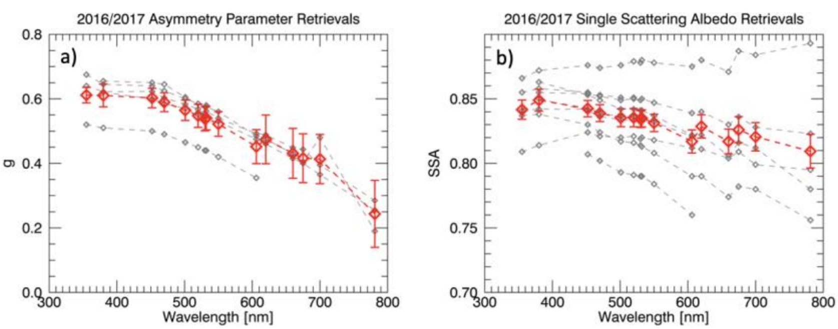

Figure 3: Retrieved a) asymmetry parameter and b) SSA spectra for 2016 and 2017 successful retrievals. The red spectrum indicates the mean retrieved values with associated error bars; the grey spectra are the individual retrievals.

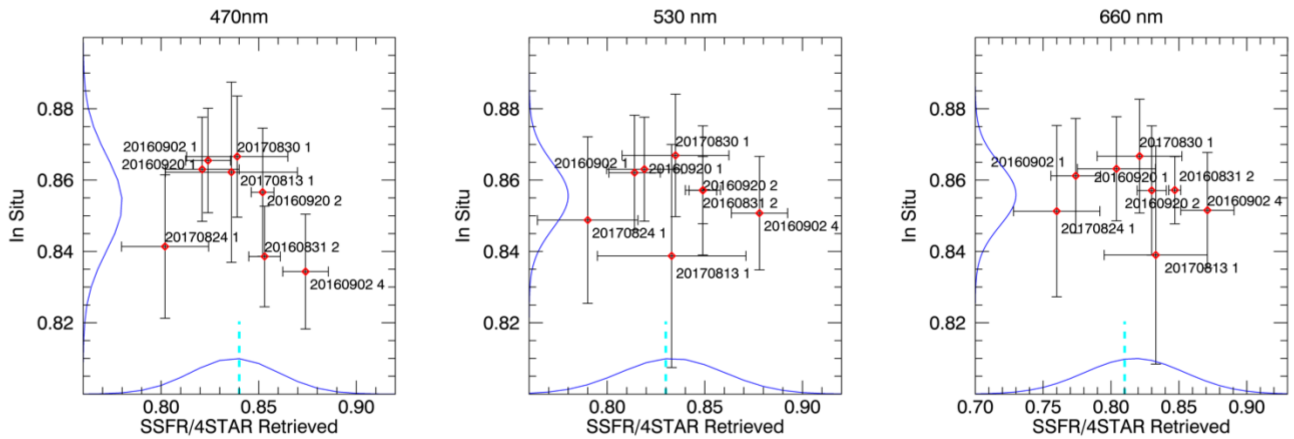

Figure 4: *In situ* vs. retrieved SSA values for a) 470 b) 530 and c) 660 nm. *In situ* values show transmittance-weighted SSA representative of the whole column, with error bars representing the standard deviation of all measured values throughout the spiral profile. *In situ* data is not available for the 20170812 case and is therefore not shown. The uncertainties for retrieved SSA for all wavelengths are provided in Appendix E. The blue dashed line indicates the values found by Davies et al. (2019).

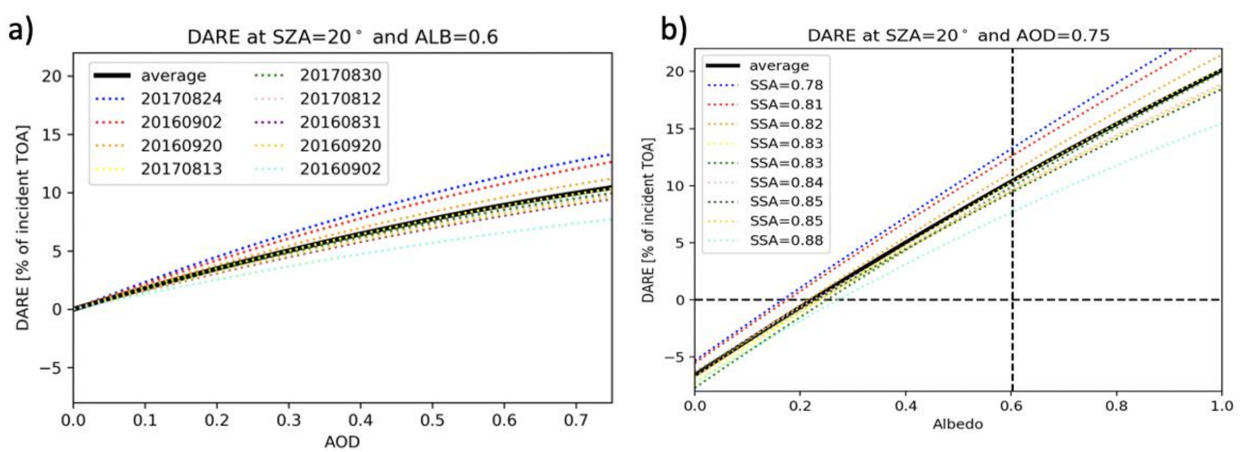

Figure 5: (a) DARE as a function of AOD for fixed underlying albedo (0.6) and SZA (20°), shown for the individual 9 cases from this study (colors) and the average (black). The average is the basic parameterization result, P_{DARE}. (b) DARE as a function of underlying albedo for a fixed AOD (0.75). The individual cases are labelled by their SSA at 550 nm (from more to less absorbing). The albedo at which the DARE changes is the critical albedo (horizontal dashed line). The vertical line marks an albedo of 0.6 for much of the ensuing discussion, which uses an AOD of 0.75, an albedo of 0.6, and a SZA of 20°. It should be noted that a 20° SZA is not representative of the mean in the region.

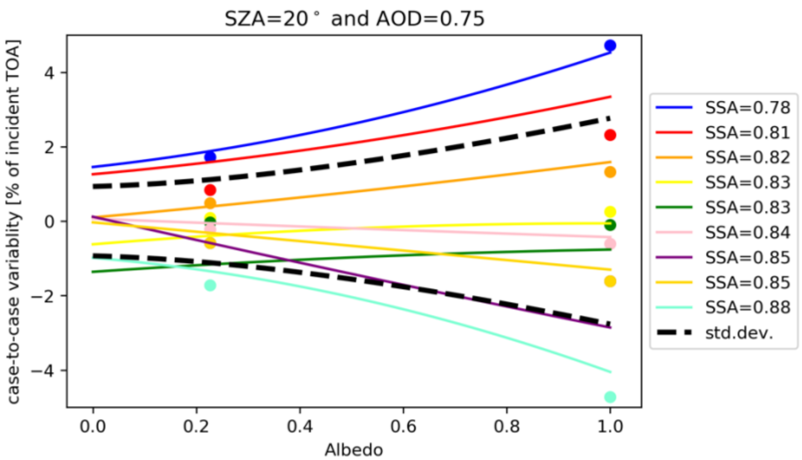

Figure 6: The difference between P_{DARE} and DARE for the individual cases at a fixed AOD (0.75) and SZA (20°). The range of variability is represented by the standard deviation (black dashed curves).

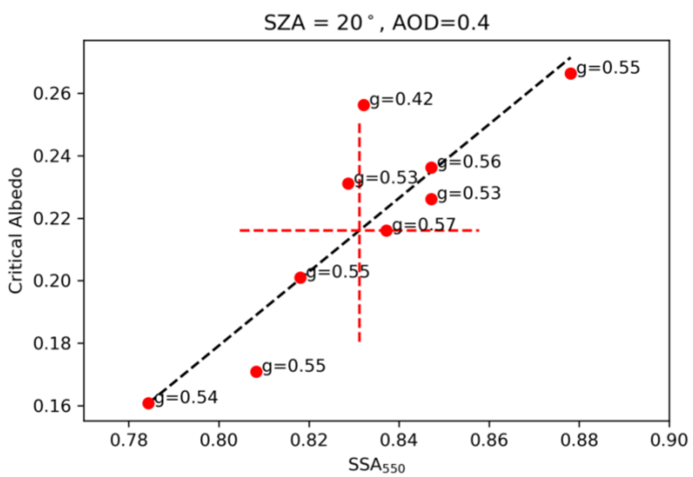

Figure 7. Critical albedo as a function of mid-visible SSA. The red dashed cross shows the case-average α_{crit}.

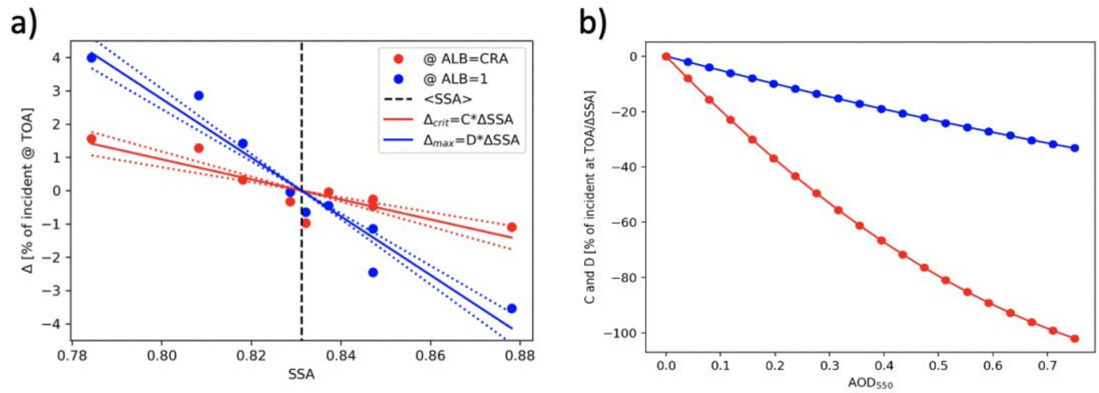

Figure 8: (a) DARE perturbations as a function of SSA at the case-average critical albedo (red) and at albedo=1 (blue) for SZA=20°. The vertical black dashed line indicates the case-average SSA. The dotted lines show the uncertainty in the C and D coefficients, which is propagated into the delta correction terms (Eq. 22 and Eq. 23). (b) the dependence of the parameters C (red curve; determined at the critical albedo (Eq. 19) and D (blue curve; determined at albedo=1 (Eq. 20) coefficients on mid-visible AOD.

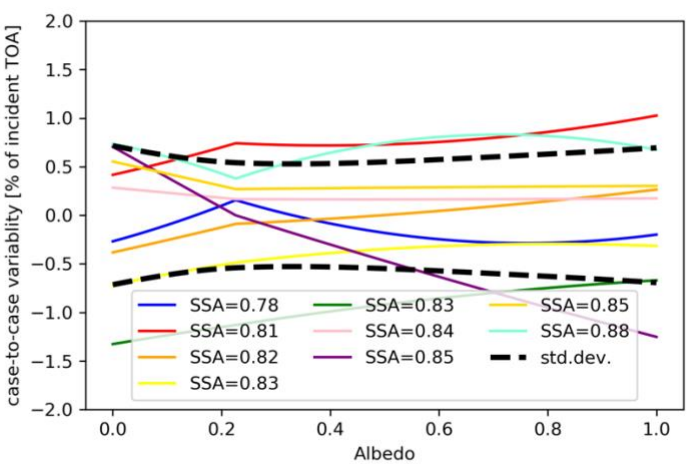

Figure 9: The difference between PX_{DARE} and P_{DARE} for 9 case SSAs at fixed AOD (0.75) and SZA (20°).

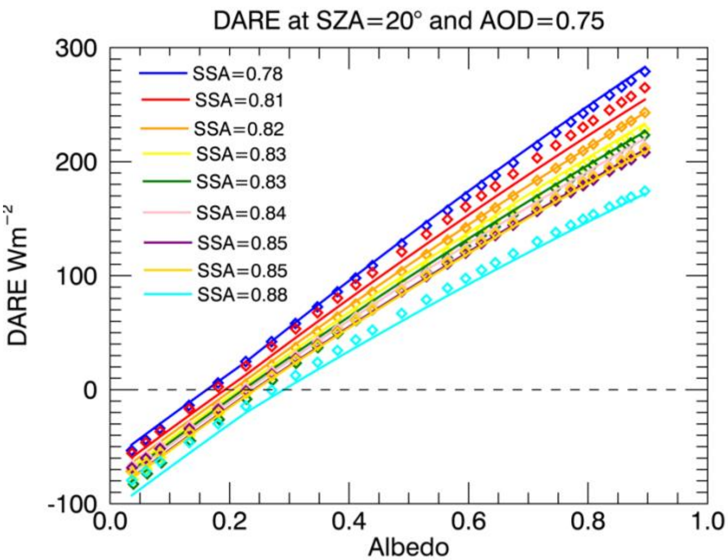

Figure 10: DARE as predicted by PX_{DARE} for the nine cases (solid lines) and DARE as calculated by the RTM (dotted colored lines).

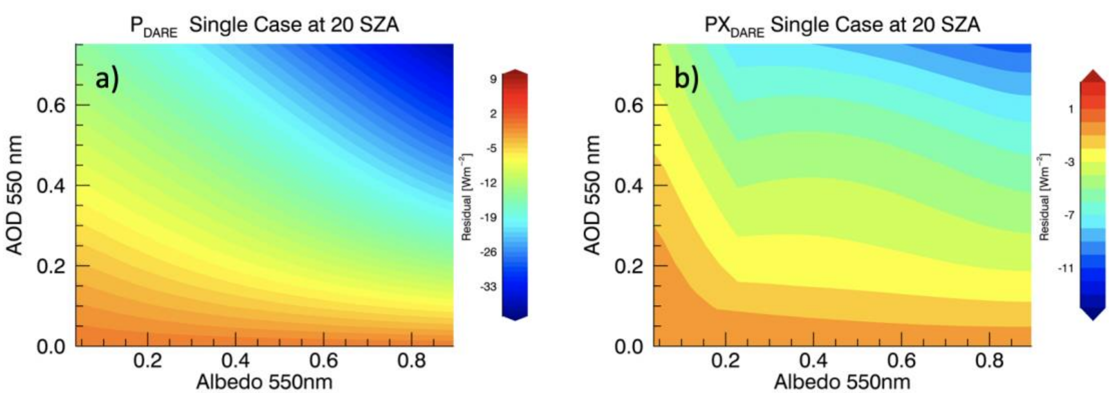

Figure 11: Residual plot of directly calculated DARE (RTM output) and predicted BB DARE values using (a)$P_{DARE}$and (b)$PX_{DARE}$for a single case at a fixed SZA (20°). Residual plots for each case can be found in Appendix D. For both figures, the residuals encompass the difference between the RTM and the P_{DARE} and PX_{DARE} parameterizations.

Date	C2: longest retrievable wavelength [nm] for which $|i| < 0.3$.	C3:AR_{∞}	Status: SSA_{λ} /g_{λ}
20160831 #1*	Fail		
20160831 #2*	550 nm	1.04	yes/yes
20160902 #1	>781nm	1.01	yes/yes
20160902 #4	>781 nm	0.98	yes/no
20160910 #1	Fail		
20160920 #1	781	1.02	yes/no
20160920 #2	781	1.07	yes/yes
20160924 #1	1627	Fail	
20160924 #3	Fail		
20160927 #1	Fail		
20170809 #1	Fail		
20170809 #2	>781	Fail**	
20170812 #1	Fail		
20170812 #3	781	1.02	yes/yes
20170813 #1*	520	1.02	yes/no
20170815 #1	675	Fail	
20170824 #1	606	1.05	yes/no

20170826 #1	355	Fail	
20170826 #3	Fail		
20170828 #1	1559	Fail**	
20170830 #1	606	1.07	yes/yes
20170831 #1	Fail		

Table 1: Retrieval Quality Metrics. Spirals are listed by date and the number in which they were performed on a particular flight. Spiral cases that did not have data spanning the entire aerosol layer are excluded from the chart (i.e. did not pass criteria #1.) The second column lists the longest wavelength for which i_λ remains below 0.3; the aerosol retrieval is only valid up to this wavelength. If i_λ at all wavelengths is greater than 0.3, the case fails completely. The third column lists the AR_∞ value. The intercept must fall between 0.9 and 1.1 to pass this metric. The right-most column provides the status for the retrieval of SSA_λ and g_λ. Cases that are analysed using the mean fit rather than the updated linear fit (update 2 from C19) are indicated by *. Cases that pass a metric but have a bad spectral shape in the albedo ratio (indicating failure) are indicated by **.

Date	UTC range	Latitude (mean)	Longitude (mean)	Cloud Albedo [500 nm]	Solar Zenith Angle	AOD [500 nm]	Column water vapor [g/cm^2]	Column ozone [DU]
20160831 #2	13:12-13:33	-17.2	7.04	0.69	37.2	0.6	1.04	289.7
20160902 #1	10:12-10:30	-15.94	8.96	0.6	28.5	0.42	1.1	342.3
20160902 #4	12:09-12:27	-15.02	8.53	0.65	26.2	0.46	1.31	341.7
20160920 #1	9:09-9:21	-16.73	10.55	0.73	33.8	0.47	0.87	410.6
20160920	11:52-	-16.68	8.9	0.45	21.2	0.57	1.15	441.9

#2	12.15							
20170812 #3	14:30-14:57	-2.9	5.04	0.57	46.7	0.32	1.37	243.8
20170813 #1	10:00-10:30	-8.97	4.95	0.7	33.6	0.21	0.41	268.8
20170824 #1	11:00-11:30	-14.9	5.1	0.54	26.4	0.27	0.77	326.2
20170830 #1	12:20-13:00	-8.05	4.91	0.49	23.2	1.36	1.6	290.9

Table 2. Spiral case details for successful aerosol retrievals. The albedo, SZA, AOD, column water vapor and column ozone are used within the radiative transfer model to retrieve aerosol properties and calculate DARE. The AOD, water vapor, and ozone are all reported above cloud.

Wavelength [nm]	355	380	452	470	501	520	530	532	550	606	620	660	675	700	781
$n_{SSA}/\ n_g$	5/3	8/5	9/5	9/5	9/5	9/5	8/5	8/5	8/5	7/4	5/3	5/3	5/3	5/3	5/3
SSA	0.84	0.85	0.84	0.84	0.84	0.84	0.83	0.83	0.83	0.82	0.83	0.82	0.83	0.82	0.81
σ_{SSA}	0.02	0.02	0.02	0.02	0.02	0.02	0.03	0.03	0.03	0.04	0.03	0.04	0.04	0.04	0.05
g	0.61	0.61	0.6	0.59	0.56	0.55	0.54	0.54	0.52	0.45	0.47	0.43	0.42	0.41	0.24
σ_g	0.08	0.06	0.06	0.06	0.06	0.06	0.06	0.06	0.06	0.06	0.01	0.02	0.02	0.06	0.05

Table 3. Mean retrieved SSA (row 3) and *g* (row 5) spectra along with their associated standard deviations (σ) (row 4, row 6, respectively). The second row provides the number of valid retrievals for that wavelength. As described in C19, individual wavelengths can fail within the retrieval resulting in fewer valid retrievals than valid cases (e.g. 355 nm SSA has 5 valid retrievals despite having 9 valid cases).

SZA	L0	L1	L2	Q0	Q1	Q2
0°	-139.4±19.1	755.9±50.4	-176.9±29.7	32.1±5.9	-270.5±29.4	130.7±18.4

10°	-140.3±19.0	748.2±49.8	-173.5±29.2	32.8±6.0	-268.9±29.1	128.6±18.2
20°	-142.8±18.9	725.2±47.9	-163.3±27.9	35.1±6.1	-264.0±28.5	122.3±17.4
30°	-146.9±18.8	687.5±44.9	-146.7±25.7	39.3±6.4	-256.6±27.3	111.7±16.2
40°	-152.5±18.4	635.9±40.6	-124.1±22.7	45.9±6.6	-247.2±25.5	97.0±14.5
50°	-158.7±17.8	570.2±35.1	-96.5±18.9	55.8±6.8	-236.5±23.0	77.9±12.4
60°	-163.2±16.7	488.8±28.6	-65.6±14.5	69.0±6.9	-223.6±19.5	54.6±9.9
70°	-158.3±15.1	385.6±21.4	-36.3±9.5	82.7±7.1	-203.6±15.0	29.2±6.9
80°	-122.2±11.9	247.9±15.6	-26.6±5.4	81.3±7.6	-162.0±10.9	17.1±3.7

Table 4a. P_{DARE} parameterization coefficients for differing SZAs. The collection of the coefficients represent the mean of all cases and the uncertainty values represent the standard deviation; the units on the *L* coefficients are W/m^2/unit optical depth; the units on the *Q* coefficients are W/m^2/(unit optical depth)^2

SZA	C1	C2	Δ_{crit} uncertainty	D1	D2	Δ_{max} uncertainty
0°	-721.8	121.5	27.0%	-2752.6	1215.3	11.4%
10°	-724.3	124.5	27.0%	-2696.1	1206.0	11.5%
20°	-733.9	126.0	26.1%	-2608.3	1178.9	11.6%
30°	-750.5	2.2	24.5%	-2463.6	1135.0	11.8%
40	-768.7	192.4	22.6%	-2263.1	1075.7	12.3%
50°	-789.2	246.3	20.5%	-2006.0	1000.8	13.0%
60°	-791.8	310.3	19.1%	-1686.5	905.8	14.3%

70°	-743.9	374.3	18.4%	-1286.6	773.6	16.8%
80°	-553.0	373.5	20.9%	-751.5	541.1	23.0%

Table 4b. PX_{DARE} additional coefficients for differing SZAs and their associated standard deviation, derived from the covariance matrix of the polynomial fits of figures 8a and 8b. These coefficients are used in Equations 22 and 23 (inserted into Equation 24) and act as extension to P in order to resolve the case-to-case variability resolvable through SSA. The units on the *C1* and *D1* coefficients are W/m^2/unit optical depth; the units on the *C2* and *D2* coefficients are W/m^2/(unit optical depth)^2. The uncertainty columns represent the relative uncertainty of the delta correction terms. These uncertainties are applicable to Equations 22 and 23, and can be further propagated into Equation 24.

Appendix A. Extension from spectral to broadband

Making the transition from the spectral to broadband is one of the main hurdles for both the parameterizations presented in this paper and for broadband DARE studies in general. Broadband DARE calculations require accurate aerosol and cloud information for all wavelengths, and it can be difficult to accurately determine the correct spectral dependence of these properties. The cloud albedo is particularly challenging since the spectral dependence depends on the SZA.

In our work, the aerosol optical properties of SSA and *g* can be retrieved for wavelengths up to 781 nm, and AOD values from 4STAR can be retrieved for up to 1650 nm. Cloud albedo is measured for the entire SSFR wavelength range, but only for a single SZA value (the mean SZA throughout the spiral time period). We therefore must a) interpolate between wavelengths and b) extend each optical property to longer wavelengths to the best of our knowledge and compute the cloud albedo for a range of SZAs.

A.1 SSA

To extend the retrieved SSA values to the remaining reported 4STAR wavelengths, we rely on the AAOD, defined as:

$$AAOD_\lambda = AOD_\lambda * (1 - SSA_\lambda). \quad (1A)$$

First, we calculate a fit line in log-log space of the AAOD for wavelengths where we have valid SSFR SSA retrievals. We extend that fit to obtain the AAOD for the remaining 4STAR wavelengths. We then re-arrange Equation 1A to determine SSA for those wavelengths where we do not have SSFR SSA retrievals. Finally, we set the SSA at wavelengths longer than 1650 nm to the mean of the longest 4STAR wavelengths, 1600 and 1650 nm. A1a illustrates the extension of SSA.

A.2 Asymmetry Parameter

Using the SSFR retrieved *g* values, we calculate a polynomial fit for the available wavelengths. We then extend the fit to longer wavelengths. Once the fit reaches 0, the remaining wavelengths are set to 0. While it would have been possible to instead use the fine mode Mie calculations (Figure B1), we chose to utilize the retrievals and approximate the fine mode, jumping to zero lacking other information. An optical closure study, though beyond the scope of this paper, is necessary. Figure A1b illustrates the extension of g.

A.3 Developing the Parameterization Grid

In order to calculate the parameterization, we grid the AOD and albedo spectra, preserving the specific spectral shapes.

A.3.1 AOD

We take the measured AOD spectrum at the BOL and multiply that spectrum by a factor to create a grid such that the values at 550 nm range from 0 to 0.75. In this way, each case has a normalized AOD grid at 550 nm while maintaining the specific spectral shape of the measured spectrum. We then extrapolate the AOD spectra to the remaining wavelengths. Figure A1c illustrates the extension and gridding of AOD.

A.3.2 Albedo

Obtaining the cloud albedo requires using the RTM to maintain accurate representation of the spectral shape. First, we retrieve the cloud properties of effective radius (Reff), and cloud optical thickness (COT) from the measured albedo using the RTM, with retrieval wavelengths of 1200 nm and 1630 nm. We then grid COT from 0 to 100 while keeping Reff constant at the retrieved value. We run the RTM to calculate a spectral albedo grid for all new pairs of Reff and COT for the range of SZAs. In these calculations, the surface for the cloud retrievals is standard Lambertian with an albedo value of 0.03. The COT range begins at 0, and this translates to a 0 "surface" albedo for the parameterization. It is acknowledged that clouds do not exhibit a Lambertian albedo. However, for irradiance calculations, the cloud albedo (non-Lambertian) can be substituted with a Lambertian albedo. Also, it is acknowledged that a sea surface is even less of a Lambertian reflector than a cloud. However, this is precisely the simplification that we made to fit both cloudy and cloud-free skies into a common framework. Since we are interested in DARE (the difference of fluxes) rather than the fluxes themselves, these simplifications should lead to only negligible effects relative to the contributing measurement uncertainties. Figure A1d illustrates the albedo grid for a single SZA.

While we extend the aerosol and cloud properties as accurately as possible, it is most crucial that the shortest wavelengths are accurate. At the longer wavelengths, the AOD becomes increasingly small, and the optical property accuracy is therefore less critical. This works in our favor since the SSFR retrieval is valid for this wavelength range where the AOD and absorption are large.

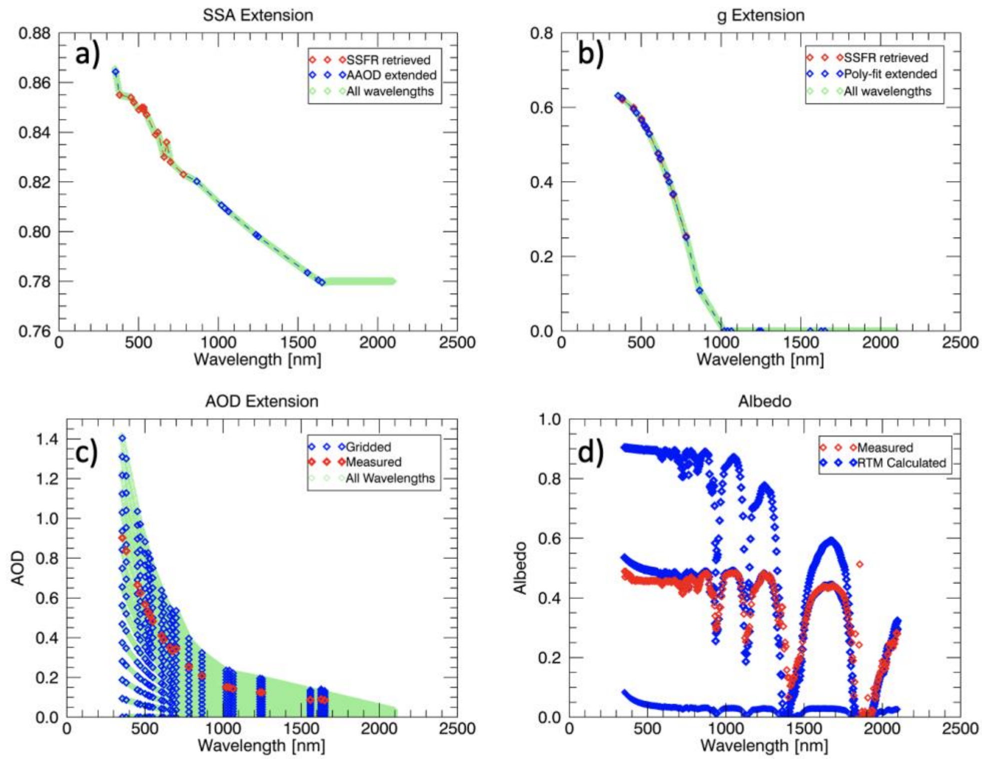

Figure A1. One example case of the extension of aerosol properties to longer wavelengths for a) SSA b) *g* and c) AOD. d) Shows the SSFR measured vs. RT-calculated albedo spectra along with the RT-calculated spectra for 0 COT and 100 COT.

Appendix B. Irradiance Retrieval

The SSFR spectral irradiance aerosol retrieval is fundamentally different than most other aerosol retrievals, which are rooted in knowledge of the aerosol size distribution along with both the imaginary and real parts of the index of refraction. These methods must utilize Mie calculations to get to the aerosol optical properties of SSA and g. As described in Pistone et al., (2019), ORACLES instrumentation such as 4STAR, the Research Scanning Polarimeter (RSP), and the Airborne Multi-angle SpectroPolarimeter Imager (AirMSPI) utilize this technique to obtain aerosol properties. The SSFR retrieval, on the other hand, circumvents the need for Mie calculations and knowledge of the size distribution or index of refraction by relying on the measured aerosol absorption itself.

However, simple Mie calculations (Figure B1) verify that a quickly decreasing asymmetry parameter is possible, and it will even decrease to 0 if no coarse mode is present. However, that is unlikely. It is more likely that the asymmetry parameter eventually goes back up again for long wavelengths - a result of even small coarse mode concentrations.

Beyond the ORACLES-specific instrumentation, AERONET stations across the globe utilize sunphotometers with the same underlying retrieval algorithms as used with 4STAR sky radiances to provide aerosol optical properties. In figure B2a and B2b, we show the mean SSFR SSA and *g* retrieval spectra compared to the nearest AERONET sites for 2016 and 2017: São Tomé, Ascension and Namibia.

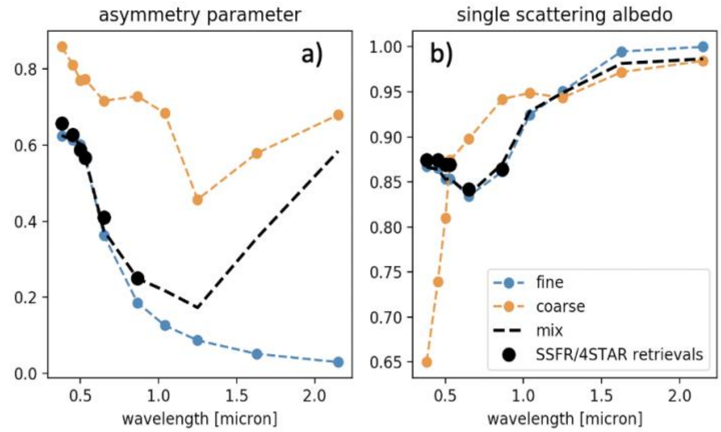

Figure B1. Mie calculations of (a) *g* and b) SSA compared to SSFR/4STAR retrieved values. The black dots show the asymmetry parameter spectrum (left) and SSA spectrum (right) as retrieved from SSFR/4STAR; the blue dot-dash line shows a fine-mode aerosol (r=0.13 micron) with real index of refraction of 1.6, and imaginary index of refraction ranging from 0.05 (380nm) to 0 (2micron); the orange dot-dash line shows a coarse-mode aerosol (r=1.3 micron) with real index of refraction of 1.6, and imaginary index of refraction ranging from 0.015 (380nm) to 0.003 (600nm) (Wagner et al., 2012); The black line shows a mix of coarse/fine aerosol (0.02:2 optical thickness ratio).

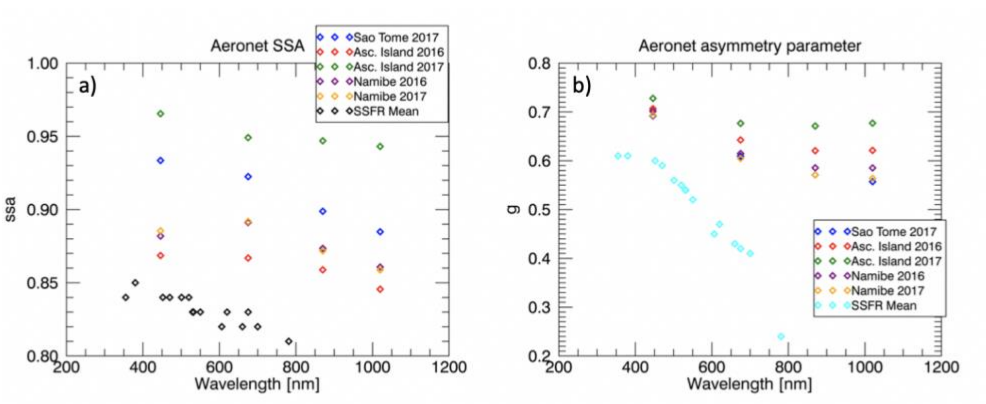

Figure B2. Retrieved values of a) SSA and b) *g* compared AERONET measured values at nearby land sites.

Appendix C. *In Situ* Transmittance Weighting

In situ SSA measurements and SSFR SSA retrievals cannot be compared directly since *in situ* SSA measurements are made continuously throughout the column (spiral), across variations in aerosol concentrations, whereas the SSFR SSA values represent a single value representative of the entire column. In order to best compare the *in situ* and retrieved SSA values, we calculate a weighted *in situ* SSA average, using a weighting function based on the transmittance through the aerosol layer.

In past studies, (e.g. C19; Pistone et al., 2019) the *in situ* SSA measurements were averaged with each SSA value weighted by its corresponding measured extinction which better represents the column SSA than a simple average. However, it is the transmittance rather than the extinction which describes the aerosols' impact on the radiation throughout the layer. Since the SSFR SSA retrieval is based on the change in radiation through the aerosol layer, it is most consistent to weigh the *in situ* measurements on transmittance rather than extinction.

For each spiral profile, we take the extinction profile as measured by the *in situ* instruments to calculate the weighting function as follows:

$$W(z) = \frac{\beta_e(z)}{\mu} e^{-\frac{\tau(z)}{\mu}} = \frac{\beta_e(z)}{\mu} t(z).$$

where $\beta_e(z)$ is the extinction, $t(z)$ is the transmittance, and $\mu = \frac{1}{cos(SZA)}$.

Figure C1 shows the *in situ* measured SSA profile for one profile case at a) 470 nm b) 530 nm and c) 660 nm. The red dashed line shows the SSFR/4STAR retrieved value; the black dashed line shows the transmittance-weighted *in situ* SSA value; the gray dashed line shows the extinction weighted *in situ* SSA value.

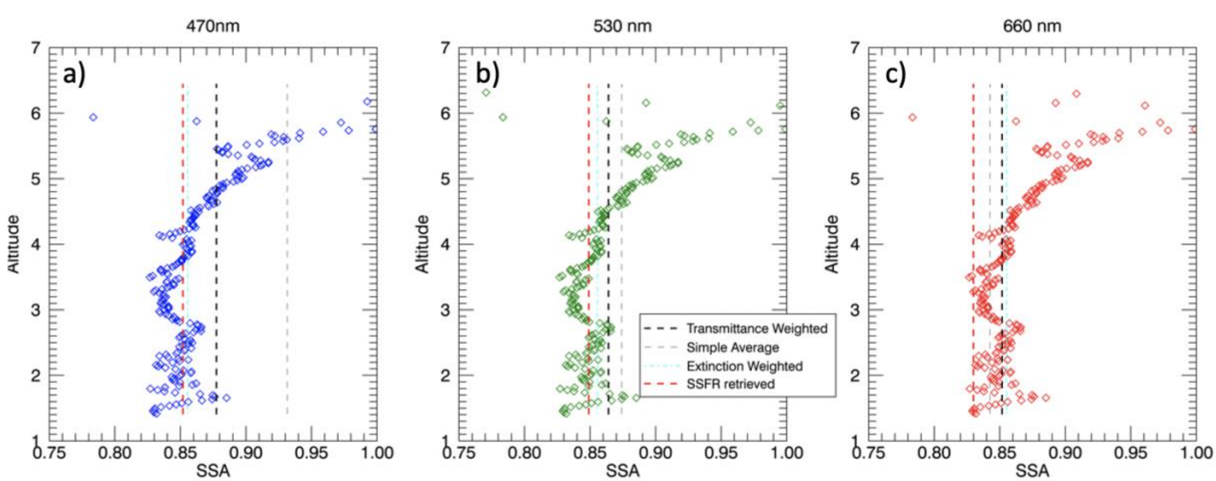

Figure C1. An example of one spiral case with the different *in situ* averages along with the SSFR retrieved SSA for a) 450 nm b) 530 nm and c) 660 nm. The colored points show the *in situ* data as measured throughout the profile.

Appendix D: Residual Figures.

Figures D1 and D2 show the residual values between directly calculated DARE (by the RTM) and DARE calculated using D1) P_{DARE} and D2) PX_{DARE} for each case. The residuals are significantly higher when using P_{DARE} vs. PX_{DARE}, illustrating that including the additional constraint of SSA (i.e. PX_{DARE}) greatly improves the parameterization performance.

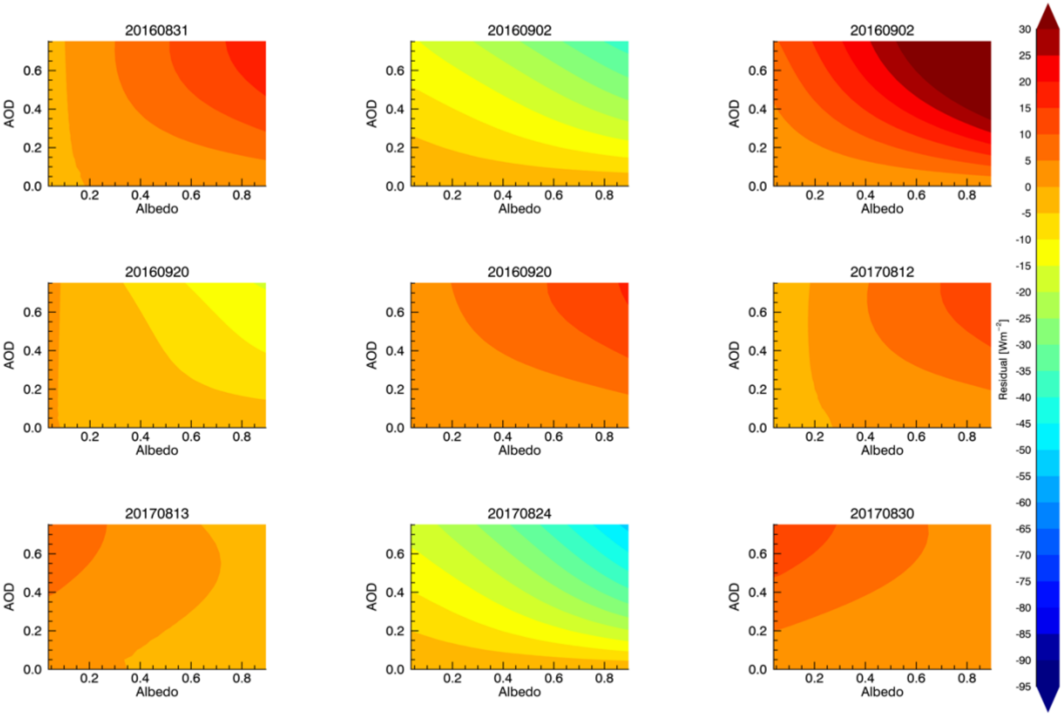

Figure D1. Residual plot of directly calculated DARE (RTM output) and predicted BB DARE values using P_{DARE} at a fixed SZA (20°).

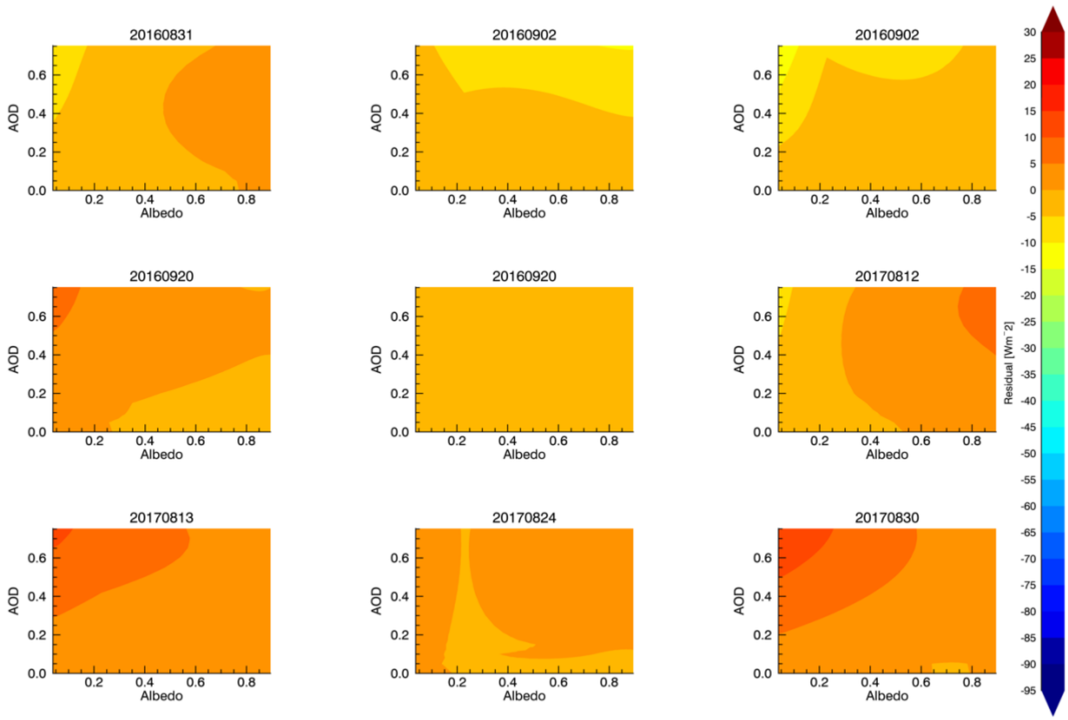

Figure D2. Residual plots of directly calculated DARE (RTM output) and predicted broadband DARE values using PX_{DARE} at a fixed SZA (20°).

Appendix E.

Retrievals of SSA and *g* for each individual case with the associated retrieval uncertainty shown as error bars. Figure E1 shows the SSA retrievals for a) 2016 and b) 2017; E2 shows both the 2016 and 2017 *g* retrievals in one figure.

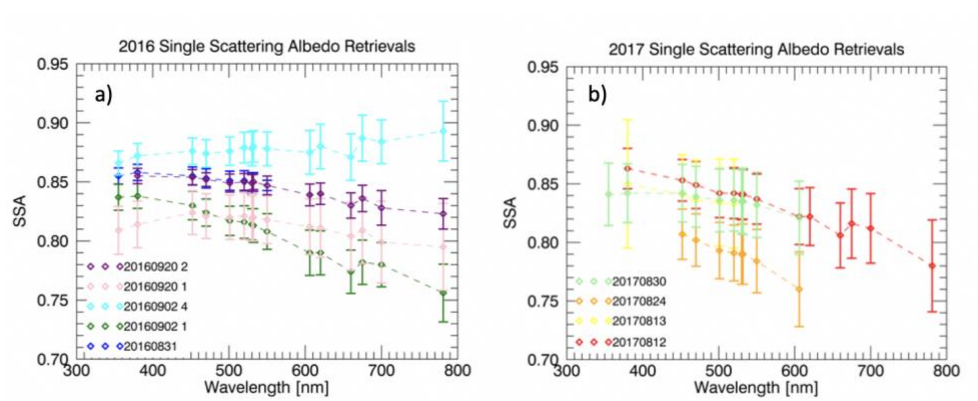

Figure E1. SSA retrievals from a) 2016 and b) 2017 with associated retrieval uncertainty.